

Measuring general relativistic dragging effects in the Earth's gravitational field with ELXIS: a proposal

Lorenzo Iorio¹

Ministero dell'Istruzione, dell'Università e della Ricerca (M.I.U.R.)-Istruzione
Permanent address for correspondence: Viale Unità di Italia 68, 70125, Bari (BA), Italy

lorenzo.iorio@libero.it

Received _____; accepted _____

Abstract

In a geocentric kinematically rotating ecliptical coordinate system in geodesic motion through the deformed spacetime of the Sun, both the longitude of the ascending node Ω and the inclination I of an artificial satellite of the spinning Earth are affected by the post-Newtonian gravitoelectric De Sitter and gravitomagnetic Lense-Thirring effects. By choosing a circular orbit with $I = \Omega = 90$ deg for a potential new spacecraft, which we propose to name ELXIS, it would be possible to measure each of the gravitomagnetic precessions separately at a percent level, or, perhaps, even better depending on the level of accuracy of the current and future global ocean tide models since the competing classical long-term perturbations on I , Ω due to the even and odd zonal harmonics J_ℓ , $\ell = 2, 3, 4, \dots$ of the geopotential ideally vanish. Moreover, a suitable linear combination of I , Ω would be able to cancel out the solid and ocean tidal perturbations induced by the K_1 tide and, at the same time, enforce the geodetic precessions yielding a secular trend of -8.3 milliarcseconds per year, thus strengthening the goal of a $\approx 10^{-5}$ test of the De Sitter effect recently proposed in the literature in the case of an equatorial coordinate system. Relatively mild departures $\Delta I = \Delta\Omega \approx 0.01 - 0.1$ deg from the ideal orbital configuration with $I = \Omega = 90$ deg are allowed. Present-day levels of relative accuracy in testing the geodetic and the gravitomagnetic effects in the field of the Sun and the Earth, respectively, are 6.4×10^{-3} (Lunar Laser Ranging) and 3×10^{-3} (Gravity Probe B) for the De Sitter precessions, and 1.9×10^{-1} for the Pugh-Schiff rates of change of gyroscopes (Gravity Probe B). Other tests of the Lense-Thirring effect with the LAGEOS type satellites are ongoing in the field of the Earth; their overall accuracy is currently debated.

keywords Experimental studies of gravity; Experimental tests of gravitational theories; Satellite orbits; Harmonics of the gravity potential field

1. Introduction

Iorio (2018) recently proposed to use a hypothetical new terrestrial artificial satellite, here dubbed¹ ELXIS and to be placed in a circular path in an orbital plane displaced by $\Omega_{\text{eq}} = 90$ deg with respect to the reference direction of the Vernal Equinox Υ perpendicularly to the Earth’s equator, in order to measure the general relativistic De Sitter effect (de Sitter 1916; Schouten 1918; Fokker 1920) on the orbital inclination I_{eq} to the equator (Iorio 2018) with a possible relative accuracy level of $\approx 10^{-5}$. A rather strict polar orbital configuration, with departures as little as $\Delta I_{\text{eq}} \approx 10^{-3} - 10^{-5}$ deg, would be required to reduce the impact of the aliasing perturbations due to the solid and ocean components of the K_1 tide, which would be one of the major sources of

¹From $\xi\lambda\xi_1\zeta$, which means ‘dragging’, ‘trailing’.

systematic errors, especially if not too high altitudes were to be adopted. The long-term rates of change of I_{eq} due to the even and odd zonal harmonics of the geopotential vanish for the orbital geometry proposed. It was tacitly assumed that the data analysis would be performed in a geocentric kinematically rotating and dynamically non-rotating (Brumberg & Kopeikin 1989; Damour, Soffel & Xu 1994; Soffel et al. 2003; Kopeikin, Efroimsky & Kaplan 2011) coordinate system having the mean Earth’s equator at the reference epoch J2000.0 as reference $\{x, y\}$ plane, and all the angular orbital elements in Iorio (2018) are to be intended as referred to it. In the standard satellite data reductions performed for a variety of purposes, a kinematically non-rotating and dynamically rotating geocentric equatorial coordinate system, the International Celestial Reference System (ICRS), is routinely used, i.e. the De Sitter precession is accounted for. It is dynamically rotating because of the fictitious forces in the satellite’s equations of motion arising from the rotation required to compensate the kinematic De Sitter precession with respect to distant quasars. They are included in the data processing algorithms in accordance with the IERS Standards (Soffel et al. 2003; Petit, Luzum & et al. 2010); see also Kopeikin, Efroimsky & Kaplan (2011, pag. 409).

In this paper, we show that, by using a² kinematically rotating geocentric coordinate system with the mean ecliptic at J2000.0 as reference $\{x, y\}$ plane, which preserves the same satellite’s orbital geometry of Iorio (2018), it is possible to suitably combine the (ecliptical) node Ω and inclination I , both affected by the De Sitter precessions (Iorio 2018), in order to cancel out, by construction, the effect of both the solid and ocean perturbations due to the K_1 tide and produce an overall De Sitter secular trend of about -8.3 mas yr^{-1} . Such a combination would be impacted neither by the zonal 055.565 tide nor by the zonals of the geopotential whose perturbations on I and Ω ideally vanish for $I = \Omega = 90 \text{ deg}$, thus enforcing the goal of reaching a $\approx 10^{-5}$ level. Furthermore, it would also be possible to analyze the node and the inclination separately to measure the general relativistic Lense-Thirring effect (Lense & Thirring 1918) affecting each of them (Iorio 2011a) to a few percent accuracy, or, in perspective, even better, depending on the accuracy of the present and future global ocean tide models adopted. The approach proposed in the present paper would allow to somewhat relax the strict conditions on I, Ω also for relatively low orbits with respect to Iorio (2018).

In putting into context the level of accuracy, in principle, obtainable with the presently proposed scenario and assessing its importance properly, the following considerations are in order. The most recent measurement of the geodetic precession was obtained with the Lunar Laser Ranging (LLR) technique (Dickey et al. 1994) for the motion of the Earth-Moon system in the field of the Sun with an accuracy level of 9×10^{-4} (Hofmann & Müller 2018). However, it is important to remark that such a figure is likely too optimistic because of an analysis of the systematic errors which might be neither reliable nor robust, as pointed out by Hofmann & Müller (2018) themselves at the end of their Sect. 4.4. Previously, Williams, Turyshev & Boggs (2004) obtained a relative accuracy of 6.4×10^{-3} level with LLR. The past Gravity Probe B

²Here and in the following, it is assumed that it is also dynamically non-rotating.

(GP-B) mission measured the geodetic precession of four orbiting man-made gyroscopes in the gravitational field of the Earth, reaching an overall relative accuracy of 3×10^{-3} in a dedicated spaceborne experiment (Everitt et al. 2011, 2015). As far as the gravitomagnetic field of the Earth is concerned, GP-B measured also the Pugh-Schiff precessions (Pugh 1959; Schiff 1960) of the onboard gyroscopes to an accuracy level of 19% (Everitt et al. 2011, 2015). At present, no aspects of the GP-B results have been criticized in the published literature; on the other hand, the obtained accuracy is not as good as the originally expected one, which was of the order of 1% (Everitt et al. 2001). Other tests of the gravitomagnetic field of the Earth have been performed in the last twenty years, and are still ongoing, with the geodetic satellites of the LAGEOS type whose Lense-Thirring orbital precessions have been measured with the Satellite Laser Ranging (SLR) technique with increasing accuracy over the years (Ciufolini et al. 2012a, 2013, 2010, 2016). Nonetheless, some aspects of them have been criticized in the literature so far, and their accuracies is the subject of a lingering debate (Ciufolini et al. 2009, 2012b; Iorio et al. 2011; Iorio 2011b, 2017; Renzetti 2012, 2013b,a, 2014b, 2015). For further planned and ongoing SLR-based investigations of the Lense-Thirring effect with the LAGEOS type satellites within the LARASE program, see Lucchesi et al. (2015); Visco & Lucchesi (2016, 2018); Pucacco & Lucchesi (2018).

The paper is organized as follows. In Section 2, a general scheme for obtaining the rates of change of the satellite’s inclination and node in the ecliptical coordinate system from the equatorial one is outlined. In Section 3, the long-term effects on I , Ω due to the general relativistic Lense-Thirring effect (Section 3.1) and the odd and even zonal harmonics J_ℓ , $\ell = 2, 3, 4, \dots$ of the Earth’s geopotential (Section 3.2) are analytically and numerically worked out. It is shown that departures of $\simeq 0.01 - 0.1$ deg from the ideal condition $I = \Omega = 90$ deg would affect the mismodelled classical precessions to less than the percent level of the gravitomagnetic ones even by assuming very conservative uncertainties in the zonals themselves. Section 4 is devoted to the tidal perturbations induced on I , Ω by the solid (Section 4.1) and ocean (Section 4.2) components of the K_1 tide for $\ell = 2$, $m = 1$, $p = 1$, $q = 0$ and their sensitivity to departures of the actual satellite’s inclination and nodes from the nominal scenario $I = \Omega = 90$ deg (Section 4.3). It is shown that the largest nominal perturbations arise from the ocean tide; depending on the accuracy of the latest global ocean tide models, their impact on the Lense-Thirring rates may be as low as a few percent. A linear combination of the precessions of I , Ω able to cancel out the K_1 tidal perturbations is designed (Section 4.4). Unfortunately, it would remove also the Lense-Thirring rates as well. In Section 5, it is shown that, instead, the De Sitter precessions are not canceled out by the aforementioned linear combination. The impact of the 3rd-body perturbations due to a distant perturber such as the Moon on both the individual precessions of the inclination and the node and their linear combination is treated in Section 6. In view of the present-day level of mismodeling in the lunar gravitational parameter, it turns out that the combined De Sitter trend would be affected, at most, at the $\simeq 3 \times 10^{-5} - 1 \times 10^{-4}$ level, while the bias on the Lense-Thirring precessions taken individually would be negligible. A cursory overview of the impact of the non-gravitational perturbations on both the individual Lense-Thirring precessions and the combined De Sitter effect is given in Section 7. By relying upon Sec. (6) of Iorio (2018) for the inclination and on several works by other researchers for the node, it turns out that, for

a geodetic satellite of LAGEOS type, their effect can be deemed as negligible with respect to the accuracy goal in the proposed relativistic tests. In Section 8, we offer a comparison with the past proposal by van Patten & Everitt (1976b) encompassing the launch of two drag-free counter-orbiting spacecraft in nearly identical circular polar orbits. Apart from being simpler and cheaper since it involves the use of a single satellite, ELXIS would be much more accurate, especially as far as the De Sitter effect is concerned. Furthermore, it would bear the possibility of increasing accuracy in forthcoming tests in view, once in orbit, of future improvements in measurement and modeling. Our findings and conclusions are resumed in Section 9. For the benefit of the reader, Appendix A displays a list of definitions of all the physical and orbital parameters used in the text, while Appendix B contains the numerical values of most of them along with the figures.

2. The rates of change of the inclination and the node in the ecliptic coordinate system

Basically, all the literature on some of the satellite orbital perturbations is developed in an equatorial coordinate system; thus, we need to devise a strategy to convert the existing analytical formulas for the equatorial rates of change of the satellite's orbital elements into expressions valid for the ecliptical coordinate system adopted here. Such an approach will turn out to be quite useful for gaining valuable information about, e.g., the tidal perturbations (see Section 4).

To this aim, let us start by rotating the normal unit vector $\hat{n} = \{\sin I \sin \Omega, -\sin I \cos \Omega, \cos I\}$ orthogonal to the orbital plane, written in terms of the ecliptical elements, from the ecliptical to the equatorial system by means of the rotation matrix

$$\mathbb{R} = \begin{pmatrix} 1 & 0 & 0 \\ 0 & \cos \epsilon & -\sin \epsilon \\ 0 & \sin \epsilon & \cos \epsilon \end{pmatrix}, \quad (1)$$

where ϵ is the obliquity. The result is

$$\hat{n}^{\text{eq}} = \{\sin I \sin \Omega, -\cos \epsilon \cos \Omega \sin I - \cos I \sin \epsilon, \cos I \cos \epsilon - \cos \Omega \sin I \sin \epsilon\}. \quad (2)$$

Then, let us calculate the node and the inclination referred to the equator from the components of Equation (2) as

$$I_{\text{eq}}(I, \Omega; \epsilon) = \arctan \left(\frac{\sqrt{(\hat{n}_x^{\text{eq}})^2 + (\hat{n}_y^{\text{eq}})^2}}{\hat{n}_z^{\text{eq}}} \right), \quad (3)$$

$$\Omega_{\text{eq}}(I, \Omega; \epsilon) = \arctan \left(\frac{\hat{n}_x^{\text{eq}}}{-\hat{n}_y^{\text{eq}}} \right). \quad (4)$$

From Equations (3) to (4) it turns out that $I, \Omega = 90 \text{ deg}$ correspond just to $I_{\text{eq}}, \Omega_{\text{eq}} = 90 \text{ deg}$. By taking the time derivatives of Equations (3) to (4), it is possible to obtain exact analytical expressions of the rates of change of $I_{\text{eq}}, \Omega_{\text{eq}}$ expressed in terms of their ecliptical I, Ω counterparts. They get simplified for $I = \Omega = 90 \text{ deg}$ reducing to³

$$\dot{I}_{\text{eq}} = \cos \epsilon \dot{I} - \sin \epsilon \dot{\Omega}, \quad (5)$$

$$\dot{\Omega}_{\text{eq}} = \sin \epsilon \dot{I} + \cos \epsilon \dot{\Omega}. \quad (6)$$

It is assumed that all the rates of changes appearing here and in the rest of the paper are averaged over the orbital period of the Earth's satellite and, when is the case, also over the period of an external third body; for the sake of simplicity, the angular brackets $\langle \dots \rangle$ denoting the average are omitted. By solving with respect to the ecliptical rates of change $\dot{I}, \dot{\Omega}$, one finally gets

$$\dot{I} = \cos \epsilon \dot{I}_{\text{eq}} + \sin \epsilon \dot{\Omega}_{\text{eq}}, \quad (7)$$

$$\dot{\Omega} = -\sin \epsilon \dot{I}_{\text{eq}} + \cos \epsilon \dot{\Omega}_{\text{eq}}. \quad (8)$$

At this stage, there is nothing left to do but to express the known formulas for $\dot{I}_{\text{eq}}, \dot{\Omega}_{\text{eq}}$ in terms of the ecliptical elements I, Ω . To this aim, it is useful to calculate $\cos I_{\text{eq}}, \sin I_{\text{eq}}, \cos \Omega_{\text{eq}}, \sin \Omega_{\text{eq}}$ entering, e.g., the amplitudes of the tidal orbital perturbations. We have

$$\cos I_{\text{eq}} = \hat{\mathbf{S}}_{\text{eq}} \cdot \hat{\mathbf{n}}^{\text{eq}} = \cos I \cos \epsilon - \cos \Omega \sin I \sin \epsilon, \quad (9)$$

$$\sin^2 I_{\text{eq}} = |\hat{\mathbf{S}}_{\text{eq}} \times \hat{\mathbf{n}}^{\text{eq}}|^2 = (\cos \epsilon \cos \Omega \sin I + \cos I \sin \epsilon)^2 + \sin^2 I \sin^2 \Omega, \quad (10)$$

$$\cos \Omega_{\text{eq}} = \frac{\cos \epsilon \cos \Omega \sin I + \cos I \sin \epsilon}{\sin I_{\text{eq}}}, \quad (11)$$

$$\sin \Omega_{\text{eq}} = \frac{\sin I \sin \Omega}{\sin I_{\text{eq}}} \quad (12)$$

In Equation (9) and Equation (10), $\hat{\mathbf{S}}_{\text{eq}}$ is the unit vector of the spin axis of the rotating primary referred to its equator.

3. The Newtonian and post-Newtonian orbital rates of change

In the following, a circular orbit with eccentricity $e = 0$ will be considered.

³They hold also by accounting for $\dot{\epsilon}$.

3.1. The post-Newtonian Lense-Thirring effect

The long-term Lense-Thirring rates of change of the inclination and the node valid in any coordinate system in which the \hat{S}_x component of the primary's symmetry axis vanishes are (Iorio 2011a)

$$\dot{I}_{\text{LT}} = \frac{2GS\hat{S}_y \sin \Omega}{c^2 a^3}, \quad (13)$$

$$\dot{\Omega}_{\text{LT}} = \frac{2GS(\hat{S}_z + \hat{S}_y \cot I \cos \Omega)}{c^2 a^3}. \quad (14)$$

In Equation (13) and Equation (14), G , c are the Newtonian constant of gravitation and the speed of light in vacuum, S is the primary's spin angular momentum, a is the semimajor axis of the test particle's orbit. It should be noted that Equation (13) and Equation (14) along with the following effects due to the geopotential (see Equations (15) to (22) below) are just a particular case of general expressions valid in a completely arbitrary coordinate system in which \hat{S} can assume any orientation in space (Iorio 2011a; Renzetti 2013c, 2014a). If an ecliptical coordinate system is adopted, it can be demonstrated that the approach outlined in Section 2 yields the same results as those obtained by Iorio (2011a); Renzetti (2013c, 2014a) for $\hat{S}_x = 0$, $\hat{S}_y = \sin \epsilon$, $\hat{S}_z = \cos \epsilon$.

Figure 1 and Figure 2 depict the agreement between Equation (13) and Equation (14) and the numerically integrated Lense-Thirring shifts which display just the expected linear temporal behaviour for the specific scenario $I = \Omega = 90$ deg (see Section 3.2 for its relevance).

3.2. The Newtonian even and odd zonal harmonics of the geopotential

The classical long-term rates of change of the node due to the first even and odd zonals of low degree are⁴ (Iorio 2011a; Renzetti 2013c, 2014a)

$$\dot{\Omega}_{J_2} = \frac{3}{2} n_b J_2 \left(\frac{R}{a}\right)^2 (\hat{S}_y \cos \Omega - \hat{S}_z \cot I) (\hat{S}_z + \hat{S}_y \cos \Omega \cot I) \sin I, \quad (15)$$

$$\dot{\Omega}_{J_3} = 0, \quad (16)$$

$$\dot{\Omega}_{J_4} = -\frac{15}{64} n_b J_4 \left(\frac{R}{a}\right)^4 (\hat{S}_z + \hat{S}_y \cos \Omega \cot I) (\hat{S}_z \cos I - \hat{S}_y \cos \Omega \sin I) \times$$

⁴Eqs. (12) to (15) of Iorio (2011a) yield Equation (19) and Equation (15) with the replacement $Q_2 \rightarrow -GMR^2 J_2$. It corrects a missing minus sign in Iorio (2011a, p. 124001-4).

$$\times \left[5 - 7\hat{S}_z^2 + (7 - 21\hat{S}_z^2) \cos 2I + 14(-1 + \hat{S}_z^2) \cos 2\Omega \sin^2 I + 28\hat{S}_y\hat{S}_z \cos \Omega \sin 2I \right], \quad (17)$$

$$\dot{\Omega}_{J_5} = 0. \quad (18)$$

The classical long-term rates of change of the inclination due to the first even and odd zonals of low degree are (Iorio 2011a; Renzetti 2013c, 2014a)

$$\dot{I}_{J_2} = \frac{3}{2} n_b J_2 \left(\frac{R}{a} \right)^2 \hat{S}_y (\hat{S}_y \sin I \cos \Omega - \hat{S}_z \cos I) \sin \Omega, \quad (19)$$

$$\dot{I}_{J_3} = 0, \quad (20)$$

$$\begin{aligned} \dot{I}_{J_4} = & \frac{15}{128} n_b J_4 \left(\frac{R}{a} \right)^4 \hat{S}_y \left\{ -\hat{S}_y (-1 + 7\hat{S}_z^2) (5 + 7 \cos 2I) \sin I \sin 2\Omega + \right. \\ & + \hat{S}_z \cos I \left[(-3 + 7\hat{S}_z^2) (1 + 7 \cos 2I) \sin \Omega - 42 (-1 + \hat{S}_z^2) \sin^2 I \sin 3\Omega \right] + \\ & \left. + 7\hat{S}_y (-1 + \hat{S}_z^2) \sin^3 I \sin 4\Omega \right\}, \quad (21) \end{aligned}$$

$$\dot{I}_{J_5} = 0. \quad (22)$$

In Equations (15) to (22), $n_b = \sqrt{\mu a^{-3}}$ is the Keplerian mean motion ($\mu = GM$ is the gravitational parameter of the primary, whose mass is M), R is the mean equatorial radius of the central body, while $J_\ell = -\sqrt{2\ell + 1} \bar{C}_{\ell,0}$, $\ell = 2, 3, 4, \dots$ are the zonal harmonic coefficients of degree ℓ of the Newtonian multipolar expansion of the primary's gravity field. The latter ones, in turn, are expressed in terms of $\bar{C}_{\ell,m}$, which are the fully normalized Stokes coefficient of degree ℓ and order m of the multipolar expansion of the gravitational potential of the central body; $m = 0$ for the zonal harmonics.

For a general value of the inclination, Equations (15) to (17) tells us that, if $\Omega = 90$ deg, the node circulates with a secular precession given mainly by

$$\dot{\Omega} \simeq -\frac{3}{2} n_b J_2 \left(\frac{R}{a} \right)^2 \hat{S}_z^2 \cos I \left[1 - \frac{5 J_4}{8 J_2} \left(\frac{R}{a} \right)^2 (-3 + 7\hat{S}_z^2 \cos^2 I) \right]. \quad (23)$$

This implies that the inclination undergoes both relativistic and classical long-periodic, harmonic variations whose frequencies are $j\dot{\Omega}$, $j = 1, 2, 3 \dots$. In particular, there are some components of Equations (19) to (22), proportional to $\hat{S}_y \hat{S}_z \cos I \sin \Omega$, which have the same temporal pattern of

Equation (13). Thus, they act as a potentially insidious systematic bias depending on the level of mismodeling in the zonal harmonics. The same holds also for Equation (14), impacted by the mismodelled part of Equation (23).

On the other hand, if the orbital plane is perpendicular to the ecliptic ($I = 90$ deg), by choosing the initial value $\Omega = 90$ deg allows to:

- (a) Keep the node rate essentially constant, as per

$$\dot{\Omega}_{J_2} = \frac{3}{2}n_b J_2 \left(\frac{R}{a}\right)^2 \hat{S}_z \hat{S}_y \cos \Omega, \quad (24)$$

$$\dot{\Omega}_{J_4} = \frac{15}{32}n_b J_4 \left(\frac{R}{a}\right)^4 \hat{S}_z \hat{S}_y \left[-1 + 7\hat{S}_z^2 + 7(-1 + \hat{S}_z^2) \cos 2\Omega\right] \cos \Omega \quad (25)$$

which are obtained from Equations (15) to (17) for $I = 90$ deg.

- (b) Maximize the Lense-Thirring rates of change which become secular trends, as per Equation (13) and Equation (14)
- (c) Cancel all the classical rates of change on the inclination due to the static part of the geopotential, as per

$$\dot{I}_{J_2} = \frac{3}{4}n_b \left(\frac{R}{a}\right)^2 \hat{S}_y^2 J_2 \sin 2\Omega, \quad (26)$$

$$\dot{I}_{J_3} = 0, \quad (27)$$

$$\dot{I}_{J_4} = \frac{15}{64}n_b \left(\frac{R}{a}\right)^4 J_4 (1 - \hat{S}_z^2) \left[-1 + 7\hat{S}_z^2 + 7(-1 + \hat{S}_z^2) \cos 2\Omega\right] \sin 2\Omega, \quad (28)$$

$$\dot{I}_{J_5} = 0, \quad (29)$$

which come from Equations (19) to (22) for $I = 90$ deg.

Figure 3, obtained by numerically integrating the equations of motion with the accelerations due to the first five zonals of the geopotential, shows that, actually, the node and the inclination stay constant to their initial values if $\Omega = I = 90$ deg are adopted for them.

In order to cope with the unavoidable orbital injection errors inducing departures from the chosen ideal orbital geometry, in Figure 4 and Figure 5 we numerically investigate the impact of offsets of the order of $\Delta\Omega = \Delta I = 0.1 - 0.01$ deg from the proposed scenario characterized by $\Omega = I = 90$ deg for different altitudes of the satellite. Since the largest contribution to the classical

inclination rate is due to J_2 , the level of mismodeling in it plays a crucial role in determining the largest admissible deviations from the nominal orbital configuration. According to Iorio (2012a), who relies upon the method proposed by Wagner & McAdoon (2012) to realistically compare geopotential harmonics in recent and past gravitational fields, a conservative evaluation of the actual uncertainty in the first even zonal points toward $\delta\overline{C}_{2,0} \simeq 3 \times 10^{-11} - 2 \times 10^{-10}$. On the other hand, the formal, statistical errors $\sigma_{\overline{C}_{2,0}}$ released in several global gravity models are as little as $\simeq 10^{-12} - 10^{-13}$. By assuming $\delta\overline{C}_{2,0} = 2 \times 10^{-10}$, Figure 1 and Figure 2 and Figure 4 and Figure 5 show that $\Delta\Omega = \Delta I = 0.01$ deg allow to reach a $\simeq 3 - 5 \times 10^{-3}$ level of systematic error in the Lense-Thirring effect for any altitude considered, while for $\Delta\Omega, \Delta I = 0.1$ deg, the bias amounts to $\simeq 3 - 5 \times 10^{-2}$. Such results show that, in the present case and contrary to other ongoing and forthcoming tests of the gravitomagnetic field of the Earth with, e.g., the LAGEOS type spacecraft, it is not so important to have a particularly accurate value of $\overline{C}_{2,0}$, at least with respect to such other contexts. Indeed, even should our choice for $\delta\overline{C}_{2,0}$ be too conservative, this could only further benefit our scenario allowing for even weaker constraints on the offsets $\Delta I, \Delta\Omega$. Thus, we can put aside certain subtleties pertaining, e.g., the different mean epochs of the geopotential models used, their time dependence, the role of the a-priori background gravity fields used in constructing the new global solutions, the different accuracies at the low degrees of the models based on GRACE and GOCE, etc. They may enter a more detailed discussion on the correct way to assess the realistic uncertainty in $\overline{C}_{2,0}$ which might be more pertinent in different tests. It is interesting to remark that the deviations from the ideal polar orbit of GP-B were as little as 5×10^{-5} deg at its launch (Kahn 2007, p. 141); our constraints are much less demanding.

In fact, the long-term geopotential perturbations bring indirectly into play another potential source of systematic error. It is the time-dependence of the Earth's spin axis because of the precession and nutation induced by the time-varying lunisolar torques, which displace \hat{S} from its orientation with respect to the mean equator and equinox of J2000.0 to the true equator and equinox (true-of-date), and the of the obliquity itself, which experiences a slight decrease, because of the gravitational pull of exerted by the other planets; see, e.g., Montenbruck & Gill (2000, Sect. 5.2). Such effects induce a non-linear time dependence on the inclination and node rates of change averaged over the satellite's orbital period which, in principle, should be taken into account in evaluating the temporal changes of I, Ω mainly due to J_2 since, as a result, they undergo additional offsets $\Delta I_{J_2}^{\hat{S}}(t), \Delta\Omega_{J_2}^{\hat{S}}(t)$ induced by the aforementioned astronomical phenomena. In particular, it is important that they can be modeled with sufficiently high precision for our accuracy goals. Since we are not interested here in, say, paleoclimatological studies spanning temporal intervals as long as Myr or Gyr, it can be done as follows. First, let us take the Earth's spin axis referred to the mean equator and equinox at J2000.0 $\hat{S}_0 = \{0, 0, 1\}$ and refer it to the mean equator and equinox of some other epoch t (mean-of-date) by means of the precession matrix \mathbb{P} . As a suitable parametrisation of it, the three angles ζ, ϑ, z can be adopted; over timescales of just some yr, they can be expressed as

$$\zeta(t) \simeq \zeta_0 + \dot{\zeta}t + \mathcal{O}(t^2), \quad (30)$$

$$\vartheta(t) \simeq \dot{\vartheta}t + O(t^2), \quad (31)$$

$$z(t) \simeq z_0 + \dot{z}t + O(t^2). \quad (32)$$

The values and the associated uncertainties of the quantities entering Equations (30) to (32) are listed in Table 2 of Appendix B. Then, the mean-of-date spin axis has to be rotated to its true-of-date orientation by means of the nutation matrix \mathbb{N} expressed in terms of the angles $\epsilon + \Delta\epsilon$, ϵ , $\Delta\psi$. About $\Delta\epsilon$, $\Delta\psi$, we will retain just their largest contributions due to the lunar node Ω_{ζ} , whose relevant values and uncertainties are displayed in Table 2 of Appendix B. Finally, we will rotate $\hat{\mathbf{S}}$ from the true-of-date coordinates, referred to the true equator and equinox, to the ecliptical coordinates by accounting for the rate of change of the obliquity as

$$\epsilon \simeq \epsilon_0 + \dot{\epsilon}t + O(t^2); \quad (33)$$

Table 2 of Appendix B collects the values and the uncertainties of ϵ_0 , $\dot{\epsilon}$. As a result, the exact long-term rates of change of I , Ω due to J_2 written in terms of \hat{S}_x , \hat{S}_y , \hat{S}_z , retrievable from Iorio (2011a, Eqs. (12) to (15)), fully account for the motion of the Earth’s spin axis. The, we integrate the Taylor expansion of $\dot{I}_{J_2}(t)$, $\dot{\Omega}_{J_2}(t)$ truncated to, say, the 3rd order in t , with respect to time obtaining analytical expressions for the time-dependent offsets $\Delta I_{J_2}^{\hat{S}}(t)$, $\Delta \Omega_{J_2}^{\hat{S}}(t)$ due to the temporal evolution of $\hat{\mathbf{S}}(t)$. Finally, we propagate the present-day errors in ϵ_0 , $\dot{\epsilon}$, ζ_0 , $\dot{\zeta}$, $\dot{\vartheta}$, z_0 , \dot{z} , $\Delta\epsilon$, $\Delta\psi$ in a root-sum-square (RMS) way by obtaining the time series of the mismodeled offsets $\sigma_{\Delta I_{J_2}^{\hat{S}}}(t)$, $\sigma_{\Delta \Omega_{J_2}^{\hat{S}}}(t)$ due to the uncertainties in the main constituents of the precession/nutation and of the change of the obliquity. Figure 6 shows $\sigma_{\Delta I_{J_2}^{\hat{S}}}(t)$, $\sigma_{\Delta \Omega_{J_2}^{\hat{S}}}(t)$ over a time span 12 yr, from 2020 to 2032, for different values of the satellite’s semimajor axis a . They were computed by using the nominal value of J_2 retrieved from some Earth’s gravity model. It turned out that the magnitude of the initial offsets ΔI_0 , $\Delta \Omega_0$ do not have a particular impact on the plots. It can be noted that, while the inclination reaches at most $\simeq 0.08$ mas for low-altitude orbits, the node is slightly more sensitive to the mismodeling in the precession/nutation and the obliquity since its shift can be as large as $\simeq 0.2$ mas for $a = 7000$ km.

4. The tidal perturbations

4.1. the solid tides

The long-term perturbations due to the solid component of the $\ell = 2$, $m = 1$, $p = 1$, $q = 0$ constituent of the tesseral tide K_1 on the satellite’s inclination and node, referred to the equator,

are

$$\dot{i}_{\text{eq}}^{K_1,s} = -\sqrt{\frac{5}{24\pi}} \frac{3g_{\oplus} R_{\oplus}^3 k_{2,1,K_1}^{(0)} H_2^1(K_1) \cos I_{\text{eq}}}{2n_b a^5} \sin(\Omega_{\text{eq}} - \delta_{2,1,K_1}), \quad (34)$$

$$\dot{\Omega}_{\text{eq}}^{K_1,s} = \sqrt{\frac{5}{24\pi}} \frac{3g_{\oplus} R_{\oplus}^3 k_{2,1,K_1}^{(0)} H_2^1(K_1) (1 - 2 \cos^2 I_{\text{eq}})}{2n_b a^5 \sin I_{\text{eq}}} \cos(\Omega_{\text{eq}} - \delta_{2,1,K_1}). \quad (35)$$

They can be calculated by applying the Lagrange planetary equations for the rates of change of the inclination and the node (Bertotti, Farinella & Vokrouhlický 2003) to Eq. (18) of Iorio (2001). In Equation (34) and Equation (35), g_{\oplus} is the Earth's acceleration of gravity at the equator, while $k_{2,1,K_1}^{(0)}$, $H_2^1(K_1)$, $\delta_{2,1,K_1}$ are the dimensionless frequency-dependent Love number, the solid tidal height, and the phase lag of the response of the solid Earth with respect to the constituent K_1 of degree $\ell = 2$ and order $m = 1$, respectively. According to Equation (7) and Equation (8), the solid K_1 -induced rate of changes of the inclination and node, referred to the ecliptic, are

$$\begin{aligned} \dot{i}^{K_1,s} = & \sqrt{\frac{5}{24\pi}} \frac{3g_{\oplus} R_{\oplus}^3 k_{2,1,K_1}^{(0)} H_2^1(K_1)}{2n_b a^5} \left[-\cos \epsilon \cos I_{\text{eq}} (\sin \Omega_{\text{eq}} \cos \delta_{2,1,K_1} - \right. \\ & \left. - \cos \Omega_{\text{eq}} \sin \delta_{2,1,K_1}) + \sin \epsilon \left(\frac{1 - 2 \cos^2 I_{\text{eq}}}{\sin I_{\text{eq}}} \right) (\cos \Omega_{\text{eq}} \cos \delta_{2,1,K_1} + \right. \\ & \left. + \sin \Omega_{\text{eq}} \sin \delta_{2,1,K_1}) \right], \end{aligned} \quad (36)$$

$$\begin{aligned} \dot{\Omega}^{K_1,s} = & \sqrt{\frac{5}{24\pi}} \frac{3g_{\oplus} R_{\oplus}^3 k_{2,1,K_1}^{(0)} H_2^1(K_1)}{2n_b a^5} \left[\sin \epsilon \cos I_{\text{eq}} (\sin \Omega_{\text{eq}} \cos \delta_{2,1,K_1} - \right. \\ & \left. - \cos \Omega_{\text{eq}} \sin \delta_{2,1,K_1}) + \cos \epsilon \left(\frac{1 - 2 \cos^2 I_{\text{eq}}}{\sin I_{\text{eq}}} \right) (\cos \Omega_{\text{eq}} \cos \delta_{2,1,K_1} + \right. \\ & \left. + \sin \Omega_{\text{eq}} \sin \delta_{2,1,K_1}) \right] \end{aligned} \quad (37)$$

in which Equations (9) to (12) are to be used to express Equation (36) and Equation (37) in terms of the ecliptical orbital elements.

An alternative approach to straightforwardly obtain Equation (36) and Equation (37) consists of expressing the perturbing tidal potential of Eq. (18) of Iorio (2001) for the solid component of K_1 with $\ell = 2$, $m = 1$, $p = 1$, $q = 0$ in terms of the ecliptical orbital elements and, then, applying the Lagrange planetary equations, which are not restricted to any coordinate system, to

them. In this way, it is also possible to straightforwardly infer that, in the case $I = \Omega = 90$ deg, the long-term perturbations due to the zonal constituent 055.565 with $\ell = 2$, $m = 0$, $p = 1$, $q = 0$ vanish for both the inclination and the node.

In the ideal case $e = 0$, $I = \Omega = 90$ deg, Equation (36) and Equation (37) become

$$i^{K_1,s} = \sqrt{\frac{5}{24\pi}} \frac{3g_{\oplus} R_{\oplus}^3 k_{2,1,K_1}^{(0)} H_2^1(K_1) \sin \delta_{2,1,K_1} \sin \epsilon}{2n_b a^5}, \quad (38)$$

$$\dot{\Omega}^{K_1,s} = \sqrt{\frac{5}{24\pi}} \frac{3g_{\oplus} R_{\oplus}^3 k_{2,1,K_1}^{(0)} H_2^1(K_1) \sin \delta_{2,1,K_1} \cos \epsilon}{2n_b a^5}. \quad (39)$$

4.2. The ocean tides

As far as the ocean component of the $\ell = 2$, $m = 1$, $p = 1$, $q = 0$ K_1 tidal line are concerned, we have

$$i_{\text{eq}}^{K_1,\text{oc}} = \frac{6G\rho_w R_{\oplus}^4 (1 + k'_2) C_{2,1,K_1}^+ \cos I_{\text{eq}}}{5n_b a^5 (1 - e^2)^2} \cos(\Omega_{\text{eq}} - \varepsilon_{2,1,K_1}^+), \quad (40)$$

$$\dot{\Omega}_{\text{eq}}^{K_1,\text{oc}} = \frac{6G\rho_w R_{\oplus}^4 (1 + k'_2) C_{2,1,K_1}^+ (1 - 2 \cos^2 I_{\text{eq}})}{5n_b a^5 (1 - e^2)^2 \sin I_{\text{eq}}} \sin(\Omega_{\text{eq}} - \varepsilon_{2,1,K_1}^+). \quad (41)$$

They can be obtained with the Lagrange planetary equations applied to Eq. (46) of Iorio (2001). In Equation (40) and Equation (41), ρ_w is the volumetric ocean water density, k'_2 is the dimensionless load Love number, while $C_{2,1,K_1}^+$, $\varepsilon_{2,1,K_1}^+$ are the ocean tidal height and the phase shift due to hydrodynamics of the oceans for the tidal constituent K_1 of degree $\ell = 2$ and order $m = 1$, respectively. From Equation (7) and Equation (8), applied to Equation (40) and Equation (41), one gets

$$i^{K_1,\text{oc}} = \frac{6G\rho_w R_{\oplus}^4 (1 + k'_2) C_{2,1,K_1}^+}{5n_b a^5 (1 - e^2)^2} \left[\cos \epsilon \cos I_{\text{eq}} \left(\cos \Omega_{\text{eq}} \cos \varepsilon_{2,1,K_1}^+ + \sin \Omega_{\text{eq}} \sin \varepsilon_{2,1,K_1}^+ \right) + \right. \\ \left. + \sin \epsilon \left(\frac{1 - 2 \cos^2 I_{\text{eq}}}{\sin I_{\text{eq}}} \right) \left(\sin \Omega_{\text{eq}} \cos \varepsilon_{2,1,K_1}^+ - \cos \Omega_{\text{eq}} \sin \varepsilon_{2,1,K_1}^+ \right) \right], \quad (42)$$

$$\dot{\Omega}^{K_1,\text{oc}} = \frac{6G\rho_w R_{\oplus}^4 (1 + k'_2) C_{2,1,K_1}^+}{5n_b a^5 (1 - e^2)^2} \left[-\sin \epsilon \cos I_{\text{eq}} \left(\cos \Omega_{\text{eq}} \cos \varepsilon_{2,1,K_1}^+ + \sin \Omega_{\text{eq}} \sin \varepsilon_{2,1,K_1}^+ \right) + \right.$$

$$+ \cos \epsilon \left(\frac{1 - 2 \cos^2 I_{\text{eq}}}{\sin I_{\text{eq}}} \right) \left(\sin \Omega_{\text{eq}} \cos \varepsilon_{2,1,K_1}^+ - \cos \Omega_{\text{eq}} \sin \varepsilon_{2,1,K_1}^+ \right) \Big]. \quad (43)$$

Also Equation (42) and Equation (43) can be alternatively obtained by expressing Eq. (46) of Iorio (2001) for the ocean component of K_1 with $\ell = 2$, $m = 1$, $p = 1$, $q = 0$ in terms of the ecliptical orbital elements and, then, using the Lagrange planetary equations.

For $I = \Omega = 90$ deg, Equation (42) and Equation (43) reduce to

$$\dot{J}^{K_1, \text{oc}} = \frac{6G\rho_w R_\oplus^4 (1 + k'_2) C_{2,1,K_1}^+ \cos \varepsilon_{2,1,K_1}^+ \sin \epsilon}{5n_b a^5}, \quad (44)$$

$$\dot{\Omega}^{K_1, \text{oc}} = \frac{6G\rho_w R_\oplus^4 (1 + k'_2) C_{2,1,K_1}^+ \cos \varepsilon_{2,1,K_1}^+ \cos \epsilon}{5n_b a^5}. \quad (45)$$

4.3. The impact of the mismodeling in the tidal parameters

Figure 7 and Figure 8 show the sensitivity of Equation (36) and Equation (37) and Equation (42) and Equation (43), plotted as functions of the satellite's semimajor axis a , to departures of I , Ω from the ideal configuration $I = \Omega = 90$ deg. By noting that the Love number $k_{2,1,K_1}$ seems currently known at an accuracy level not better than⁵ $\simeq 10^{-3}$, it turns out that not too large offsets $\Delta\Omega$, $\Delta I \simeq 0.05$ deg would be adequate to cope with the solid tidal perturbation; suffice it to say that, for GP-B, it was $\Delta I_{\text{eq}} = 5 \times 10^{-5}$ deg at its launch (Kahn 2007, p. 141). On the other hand, the nominal ocean tidal perturbations are larger than the solid ones; such a discrepancy is due to the different values of their lag angles $\delta_{2,1,K_1}$, $\varepsilon_{2,1,K_1}^+$ so that, while $\sin \delta_{2,1,K_1} \simeq -0.005$, on the other hand it is $\cos \varepsilon_{2,1,K_1}^+ \simeq 0.77$. Thus, the present-day level of uncertainty in the ocean tidal height coefficient of K_1 is of crucial importance to assess the level of aliasing which could be induced on the relativistic signatures. If one had to rely upon the old EGM96 model along with its 4×10^{-2} relative uncertainty in $C_{2,1,K_1}^+$ (Lemoine et al. 1998), the bias on the Lense-Thirring signature would be at a $\simeq 40 - 50\%$ level. However, several other global ocean tide models have been produced since then: CSR4.0 (Eanes & Schuler 1999) TPXO.6.2 (Egbert & Erofeeva 2002) GOT99 (Ray 1999) FES2004 (Lyard et al. 2006), EOT11a (Savcenko & Bosch 2012), EOT11ag (Mayer-Gürr et al. 2012). By a comparison among them, it does not seem unrealistic to assume a present-day relative uncertainty of the

⁵L. Petrov and R. Ray, personal communications, August 2018. Nonetheless, in Jagoda et al. (2018) a relative uncertainty as little as 3×10^{-4} was reported on a generic k_2 Love number determined with the LAGEOS and LAGEOS II satellites.

order of $\approx 10^{-3}$ for $C_{2,1,K_1}^+$. Indeed, by calculating mean and standard deviation of the values computed at <https://bowie.gsfc.nasa.gov/ggfc/tides/harmonics.html> from the models TPXO.6.2 (Egbert & Erofeeva 2002), GOT99 (Ray 1999) and FES2004 (Lyard et al. 2006), a relative uncertainty of 1.8×10^{-3} is inferred. It would yield an aliasing level of the Lense-Thirring signatures of a few percent.

4.4. The linear combination approach

At first sight, a possible way to overcome such an issue would consist of suitably designing a linear combination of the satellite's inclination and node which, by construction, cancels out both the ocean and solid tidal perturbations due to the K_1 line. By means of Equation (44) and Equation (45) it is possible to obtain

$$f \doteq \dot{I} + c_1 \dot{\Omega}, \quad (46)$$

with

$$c_1 = -\tan \epsilon = -0.433547. \quad (47)$$

Unfortunately, the linear combination of Equation (46) cancels out also the Lense-Thirring precessions; indeed, Equation (13) and Equation (14) reduce just to

$$\dot{I}_{\text{LT}} = \frac{2GS \sin \epsilon}{c^2 a^3}, \quad (48)$$

$$\dot{\Omega}_{\text{LT}} = \frac{2GS \cos \epsilon}{c^2 a^3} \quad (49)$$

for $e = 0$, $I = \Omega = 90$ deg. It is a consequence of a general result about f which can be drawn for $I = \Omega = 90$ deg for the perturbations induced by any disturbing acceleration. Indeed, from Equation (7) and Equation (8) and Equation (46) and Equation (47), it turns out that the combined signature for the inclination and node rates of change due to a generic perturbing acceleration A_{pert} of whatsoever physical origin, is

$$f^{\text{pert}} = \frac{j_{\text{eq}}^{\text{pert}}}{\cos \epsilon}, \quad (50)$$

where the analytical expression for $j_{\text{eq}}^{\text{pert}}$ has to be evaluated for $I = \Omega = 90$ deg. In the case of the Lense-Thirring effect, Equation (50) tells us immediately that f^{LT} vanishes since there is no gravitomagnetic precession for I in the equatorial coordinate system.

5. The De Sitter precessions

On the other hand, Equation (46) and Equation (47) have the advantage of returning a non-vanishing effect due to the post-Newtonian gravitoelectric De Sitter precessions of the satellite's inclination and node.

Indeed, by using Eq. (4) and Eq. (8) of Iorio (2018), which describe the geodetic rates of change of the satellite’s inclination and node with respect to any⁶ coordinate system, in the scenario $I = \Omega = 90$ deg, Equation (46) and Equation (47) return

$$f^{\text{DS}} = -\frac{3\mu_{\odot}n_{\oplus}^{\oplus}(\cos \Omega_{\oplus} \sin I_{\oplus} + \cos I_{\oplus} \tan \epsilon)}{2c^2a_{\oplus}(1 - e_{\oplus}^2)} = -8.31986 \text{ mas yr}^{-1}. \quad (51)$$

In Equation (51), $\mu_{\odot} = GM_{\odot}$ is the Sun’s gravitational parameter, a_{\oplus} , e_{\oplus} are the semimajor axis and the eccentricity of the heliocentric Earth’s orbit, respectively, n_{\oplus}^{\oplus} is the Keplerian mean motion of the Earth’s orbit, while I_{\oplus} , Ω_{\oplus} are the inclination and the node of the Earth’s orbit referred to the ecliptic, respectively. The signature of Equation (51) is essentially a secular trend since the inclination and the node of the heliocentric Earth’s orbit change over timescales of the order of $\simeq 0.1 - 1$ Myr, as can be inferred by their extremely slow rates of change (Murray & Dermott 2000). It is important to remark that Equation (51) would not be affected, by construction, by the largest and most insidious among the tidal perturbations, i.e. the K_1 tide; the zonal tide 055.565 is of no concern since in Section 4 it was shown that its long-term perturbations vanish for both the inclination and the node. Furthermore, also the static part of the geopotential would be of no concern, as previously shown in Section 3 for the inclination and the nodes taken separately. Figure 9 shows the impact of departures $\Delta I = \Delta \Omega = 0.1$ deg from the condition $I = \Omega = 90$ deg on the nominal zonals perturbations combined according to Equation (46) and Equation (47). The corresponding mismodeled signatures would be completely negligible even by assuming very conservative levels of uncertainty in J_{ℓ} , $\ell \geq 2$. Figure comboNUT shows that the uncertainties in the precession/nutation parameters and in the obliquity do not affect the combination of Equation (46). Indeed, it turns out that, over 12 yr, the combined mismodeled shift ranges from just 0.003 mas ($a = 7000$ km) to 0.0006 mas ($a = 14000$ km).

6. The 3rd-body perturbations: the Sun and the Moon

The results of Iorio (2012b) concerning the rates of change of the satellite’s orbital elements, averaged over its orbital period P_b , induced by a distant perturber X can be straightforwardly used in the present context since they are valid in any coordinate system. The doubly averaged rate of change of the node can be obtained by averaging Eq. (9) of Iorio (2012b) over the orbital period P_X of the 3rd-body. The general result is

$$\dot{\Omega}^{\text{3rd body}} = -\frac{3\mu_X}{8a_X^3 \sqrt{1 - e^2}(1 - e_X^2)^{3/2}n_b} [\cos I_X \cot I + \cos(\Omega - \Omega_X) \sin I_X] \times$$

⁶It is understood that it has to be intended as kinematically rotating (Brumberg & Kopeikin 1989).

$$\begin{aligned} & \times \left\{ - \left(-2 - 3e^2 + 5e^2 \cos 2\omega \right) [\cos I_X \sin I - \cos I \cos (\Omega - \Omega_X) \sin I_X] - \right. \\ & \left. - 5e^2 \sin I_X \sin 2\omega \sin (\Omega - \Omega_X) \right\}. \end{aligned} \quad (52)$$

In Equation (52), ω is the argument of pericenter of the satellite's orbit referred to the ecliptic, while μ_X , a_X , e_X , I_X , Ω_X are the gravitational parameter, the semimajor axis, the eccentricity, the inclination, the node of the body X, respectively. In the present context, I_X , Ω_X are to be meant as referred to the ecliptic. Eq. (20) of Iorio (2018) and Equation (52), for $e = 0$, $I = \Omega = 90$ deg, reduce to

$$j^{\text{3rd body}} = \frac{3\mu_X \sin^2 I_X \sin 2\Omega_X}{8a_X^3 (1 - e_X^2)^{3/2} n_b}, \quad (53)$$

$$\dot{\Omega}^{\text{3rd body}} = -\frac{3\mu_X \sin 2I_X \sin \Omega_X}{8a_X^3 (1 - e_X^2)^{3/2} n_b}, \quad (54)$$

which can be linearly combined according to Equation (46) and Equation (47) giving

$$f^{\text{3rd body}} = \frac{3\mu_X \sin I_X \sin \Omega_X (\sin I_X \cos \Omega_X + \tan \epsilon \cos I_X)}{4a_X^3 (1 - e_X^2)^{3/2} n_b}. \quad (55)$$

As far as the Moon is concerned, its node Ω_{ζ} , referred to the ecliptic, undergoes a secular precession with a period of $T_{\Omega_{\zeta}} = 18.6$ yr; its current value is $\Omega_{\zeta} = 125.1$ deg. Thus, although at the price of a long wait, Equations (53) to (55) will finally average out in view of their frequencies $\dot{\Omega}_{\zeta}$, $2\dot{\Omega}_{\zeta}$, and it can be stated that they would be of no concern for either the individual Lense-Thirring precessions of Equation (13) and Equation (14) and the combined De Sitter effect of Equation (51). Such a conclusion is true for each of the gravitomagnetic signatures also without waiting for the completion of a full cycle of the lunar node, as it can be easily checked by inspecting the maximum values of the mismodeled parts of Equation (53) and Equation (54) for any value of a and comparing them to Figure 1 and Figure 2. To this aim, we assumed a relative uncertainty in the selenocentric gravitational parameter $\mu_{\zeta} = GM_{\zeta}$ of 2×10^{-8} , as per the Object Data Page of the Moon provided by the JPL HORIZONS Web interface, revised on 2013. The situation is subtler for the combined De Sitter trend in view of the higher level of accuracy pursued. The maximum impact on Equation (55) occurs when $\Omega_{\zeta} = 90$ deg, so that

$$f_{\text{max}}^{\zeta} = \frac{3GM_{\zeta} \tan \epsilon \sin 2I_{\zeta}}{8a_{\zeta}^3 (1 - e_{\zeta}^2)^{3/2} n_b}. \quad (56)$$

In Equation (56), I_{ζ} is the inclination of the geocentric lunar orbit to the ecliptic, while a_{ζ} , e_{ζ} are the semimajor axis and the eccentricity of the geocentric Moon's orbit, respectively. In

Figure 11 we plot the mismodeled part of Equation (56) as a function of a . It can be noted that it stays in the range $\simeq 3 - 10 \times 10^{-5}$ of Equation (51).

About the 3-body effect of the Sun, it is completely negligible. Indeed, it is

$$f_{\max}^{\odot} \simeq \frac{M_{\odot}}{M_{\zeta}} \left(\frac{a_{\zeta}}{a_{\oplus}} \right)^3 \frac{\sin 2I_{\oplus}}{\sin 2I_{\zeta}} f_{\max}^{\zeta} = 3 \times 10^{-4} f_{\max}^{\zeta}. \quad (57)$$

Furthermore, the heliocentric gravitational parameter is currently known with a relative accuracy of 7×10^{-11} (Pitjeva 2015).

7. The non-gravitational perturbations

The long-term rates of change induced by the non-gravitational accelerations on the inclination and node, referred to the equator, of the LAGEOS-type satellites have been extensively investigated in the literature in the context of their bias on the equator-referred Lense-Thirring node precession by finding them at the percent level or less for LAGEOS. Thus, it is arguable that the same holds also when they are combined according to Equation (7) and Equation (8) in order to yield their ecliptical counterparts. Indeed, the averaged node perturbations which vanish for $e = 0$, $I = \Omega = 90$ deg are those due to the Poynting-Robertson effect (Lhotka, Celletti & Galeš 2016, p. 608), the infrared radiation pressure of the Earth (Sehna 1981, p. 176), the atmospheric drag (Milani, Nobili & Farinella 1987, p. 103), the hypothetical asymmetric reflectivity (Lucchesi 2002, Eq. (44), p. 1083), the geomagnetic field, as can be inferred by integrating the Gauss equation for the rate of change of the node by means of Abdel-Aziz & Khalil (2014, Eq. (24), p. 592), with $1/\sin f$ in its first term corrected to $\sin f$, to zero order in e for $I = 90$ deg, the secular trend due to the Yarkovsky-Rubincam effect (Lucchesi 2002, Eq. (19), p. 1075), the Earth albedo (Lucchesi 2001, Eq. (35), p. 456) and the solar radiation pressure (Lucchesi 2001, Eq. (18), p. 451) in absence of eclipses. In the case of eclipses, by using the first term in the series of Eq. (2) and Eq. (4) in Ferraz Mello (1972) for the shadow function it can be shown that, to zero order in e , the node rates due to the albedo and the solar radiation pressure do not vanish; nonetheless, they turn out to be proportional to $\sin 2\lambda_{\odot}$, which averages out after 1/2 yr. About the long-term signatures due to the Yarkovsky-Rubincam effect having the frequencies $\dot{\Omega}$ (Lucchesi 2002, Eq. (18), p. 1075) and $2\dot{\Omega}$ (Lucchesi 2002, Eq. (17), p. 1075), they vanish if the satellite's spin axis is perpendicular to the Earth's equator. The same holds for the secular rate due to the Yarkovsky-Schach effect (Lucchesi 2002, Eq. (34), p. 1079). A similar situation occurs for the inclination, as shown in Sec. (6) of Iorio (2018).

As far as the De Sitter effect is concerned, by recalling the general result of Equation (50), all the findings of Sec. (6) of Iorio (2018) retain their validity, pointing towards an impact of the non-gravitational perturbations on the combined De Sitter trend of Equation (51) globally meeting our requirement.

We stress that the aforementioned considerations are to be deemed just as very preliminary

because they are based on previous results with the existing LAGEOS type satellites. To this aim, it is important to remark that the architecture of, say, LAGEOS and LAGEOS II is a very old one and have several drawbacks. Just to mention a few of them, in view of the particular distribution of their corner cube retroreflectors (CCR), in practice, the satellites do not behave like a perfect sphere. Moreover, the virtual reflection point is not the center of mass of each satellite. A forthcoming, dedicated paper will be devoted to their consideration for the proposed new spacecraft ELXIS. This is particularly important for those thermal thrust forces which need the knowledge of the spin rate and orientation of the probe.

8. A comparison with the counter-orbiting scenario by van Patten and Everitt

Some decades ago, it was proposed by van Patten and Everitt (vPE) to launch a pair of counter-orbiting drag-free spacecraft in nearly identical circular and polar orbits at an altitude of about 800 km to perform a $\approx 1\%$ measurement of both the Lense-Thirring and De Sitter node precessions by monitoring the sum of their nodes (van Patten & Everitt 1976b,a; Schaechter et al. 1977; van Patten et al. 1978). In addition to the drag-free apparatus to counteract the non-gravitational perturbations, the vPE's satellites should have been endowed also with the capability of reciprocal Doppler tracking at mutual encounters when passing over the poles. Careful arrangements to avoid in-orbit collisions would have been required as well (Schaechter et al. 1976). The main, striking differences between ELXIS and the vPE's proposal are as follows

- a) The ELXIS concept is based on just a single satellite instead of two spacecraft, as in the vPE's proposal.
 - a^I) ELXIS should not be necessarily too complex and/or expensive since a comparatively simpler, well manufactured cannonball geodetic satellite of LAGEOS-type would likely fit our accuracy requirements since, as we have demonstrated, most of the non-gravitational perturbations vanish or average out after more or less long temporal intervals. Moreover, once in orbit, ELXIS could well wait for forthcoming improvements in both the tracking accuracy and in dynamical modeling of, e.g., the ocean tides, thus by allowing for repeated tests with likely continuously improved accuracy over the subsequent years.
 - a^{II}) There are no particular limitations on the orbital height, which can be conveniently set according to the unavoidable engineering/budgetary trade-off.
 - a^{III}) There are no collision-related issues.
 - a^{IV}) No careful satellite-to-satellite measurements of the angle between the two orbital planes at the poles are present.
 - a^V) The overall data analysis process of ELXIS would be much easier and less expensive than that encompassing two satellites.

- b)* While van Patten & Everitt (1976b) proposed to make a combined Lense-Thirring + De Sitter test, ELXIS would allow to perform separate-and even redundant-measurements of such two general relativistic effects. The De Sitter effect can be disentangled from the Lense-Thirring one both in the equatorial and in the ecliptical coordinate systems. Indeed, in the first case (Iorio 2018), based on the analysis of the satellite’s inclination only, the Lense-Thirring rate of change of it vanishes for $\hat{S}_x = \hat{S}_y = 0$, while in the second case, the linear combination of Equation (46) and Equation (47) cancels out just the gravitomagnetic precessions and enforces the geodetic ones yielding Equation (51). Conversely, the Lense-Thirring measurements could be easily made independently of the geodetic effect itself simply by using an ecliptical version of the standard kinematically non-rotating and dynamically rotating geocentric coordinate system in which the De Sitter precession is automatically accounted for, not showing up in spacecraft motions. Basically, it would be just a geometrically rotated version of the usual ICRS adopted for routinely analyzing Earth’s satellites data.
- c)* With ELXIS, the accuracy in measuring the De Sitter combined precessions, independently of the Lense-Thirring effect, would be of the order of $\approx 10^{-5}$, while (van Patten & Everitt 1976b) claimed a $\approx 1\%$ accuracy in a mixed measurement of both the Lense-Thirring and the geodetic precessions. On the other hand, van Patten & Everitt (1976a) wrote that they could have obtained an independent test of the De Sitter effect at 10%, i.e. about 4 orders of magnitude worse than what could be obtained with ELXIS.
- d)* The orbit injection errors on the nodes Ω of the vPE’s satellites should have been of the order of 0.03 deg (van Patten & Everitt 1976a), which is a figure comparable with the ELXIS case, although offsets up to 0.1 deg would not compromise our accuracy goals. On the other hand, the requirements by van Patten & Everitt (1976a) on the inclinations of the orbital planes would have been of the order of ≈ 0.0008 deg, while for ELXIS they are at the $\approx 0.01 - 0.1$ deg level.
- e)* A major drawback of the error budget of van Patten & Everitt (1976b,a) is, perhaps, that they seemingly did not take into account the perturbations due to the ocean tides induced on the satellites’ motions by the free space tidally distorted Earth’s potential. It is difficult to think that, say, the K_1 tide may have had no substantial effects on the vPE’s spacecraft in view of the results obtained in the present study and of the fact that, at the time of van Patten & Everitt (1976b,a), the first, relatively rudimentary satellite-based global ocean tide models, if any, are much less accurate than now. Suffice it to say that Felsentreger, Marsh & Agreen (1976) released errors in ocean tidal height $C_{2,1,K_1}^+$ as large as $\approx 8 - 28\%$. Moreover, the uncertainty in it from the global Earth’s gravity field model GEM-T3S (Lerch et al. 1992), published about 15 yr after the vPE’s proposal, was still 6%. As a consequence, the claimed $\approx 1 - 10\%$ accuracy levels claimed by van Patten & Everitt (1976b,a) might have been somewhat optimistic.

Thus, it is clear that, even by limiting ourselves to the point *a)* and assuming hypothetically the

same accuracy goals, ELXIS should be deemed as more advantageous than the vPE’s proposal. Moreover, even by pessimistically surmising that our evaluation of the actually obtainable accuracy on the De Sitter measurement should be moved to, say, the $\approx 10^{-4}$ level, it would still be 3 orders of magnitude better than 10% (van Patten & Everitt 1976a).

9. Summary and conclusions

Using a geocentric kinematically rotating ecliptical coordinate system to analyze the data of a single Earth’s satellite, provisionally named ELXIS, placed in a circular orbit perpendicular to the equator and to the reference direction of the Vernal Equinox has the advantage of allowing to use both its inclination and node to measure the general relativistic Lense-Thirring and De Sitter effects without being impacted by the competing classical long-term precessions due to the even and odd zonals of the geopotential, which ideally vanish. On the other hand, the ocean component of the K_1 tide induces aliasing perturbations which may degrade the accuracy of the proposed recovery of the individual gravitomagnetic and geodetic signatures. Depending on the actual mismodeling in the global ocean tide models, their impact on each of the Lense-Thirring rates may be at the percent level, representing the most limiting factor in measuring them. It is not unrealistic to expect further improvements in the forthcoming global tide solutions; in any case, once the satellite is in orbit, it would always be possible to wait just enough for the tidal models to reach the required accuracy. Moreover, it should be recalled that, after all, the accuracy of GP-B is 19%. Other tests of the gravitomagnetic field of the Earth performed with the existing LAGEOS type satellites have been reported in the literature, but, contrary to GP-B, they are still somewhat controversial, especially as far as the actual accuracy reached. As far as the De Sitter effect is concerned, currently known at the $\approx 10^{-3}$ level from LLR and GP-B, the goal of a $\approx 10^{-5}$ accuracy of its measurement can be enforced with respect to an equatorial frame by linearly combining its geodetic precessions on the satellite’s inclination and node in such a way to cancel out, by construction, the solid and tidal perturbations due to the K_1 and other tides. The impact of the combined 3rd-body perturbations due to the Moon, which are relevant only for the De Sitter test at the considered level of accuracy, averages out after 18.6 yr since the smallest characteristic frequency of their combined signatures is just that of the lunar node. However, given the current level of uncertainty in the selenocentric gravitational parameter, the largest bias during a full cycle of it would be no larger than $\approx 3 \times 10^{-5} - 1 \times 10^{-4}$. The non-gravitational perturbations, preliminarily examined by assuming a cannonball geodetic satellite of LAGEOS-type, should not be a concern. However, these are just preliminary guesses based on past studies in the literature performed for the existing LAGEOS type satellites, whose physical structure is quite old and pose certain drawbacks which should be overcome with an entirely new spacecraft. A dedicated, forthcoming paper will be devoted to the non-conservative forces acting on ELXIS, especially the thermal thrusts which crucially depend on the spin rate and orientation of the spacecraft. Such conclusions hold substantially for any value of the satellite’s semimajor axis and for departures as large as $\approx 0.01 - 0.1$ deg from the ideal orbital geometry proposed. Finally, we note that we

worked in an analytical way by using the Keplerian orbital elements for the sake of simplicity and clarity about the rationale of the proposed experiment, and in order to offer to the reader a preliminary error budget easy to understand. If, on the one hand, long time series of some orbital elements have been actually used so far in the performed tests of the Lense-Thirring effect with the LAGEOS type satellites, on the other hand, a more robust and reliable approach would consist of explicitly modeling the features of motion one is interested in and estimating one or more dedicated solve-for parameters in the data reduction by inspecting their correlations with the other determined parameters in the full covariance matrix. It is hoped that the present paper will boost further investigations by other researchers who may want to complement it with full covariance analyses implying numerical data simulations and reductions for, say, one or more types of spacecraft.

Acknowledgements

I am grateful to S. Kopeikin for some important clarifications and to an anonymous referee for the idea of comparing the present proposal with a past one. Also the critical remarks by three other anonymous referees were much appreciated.

Appendix A Notations and definitions

Here, some basic notations and definitions used in the text are presented (Brumberg 1991; Bertotti, Farinella & Vokrouhlický 2003; Capitaine, Wallace & Chapront 2003; Petit, Luzum & et al. 2010; Kopeikin, Efroimsky & Kaplan 2011; Poisson & Will 2014; Liu & Capitaine 2017). For the numerical values of some of them, see Tables 1 to 2. The orbital elements referred to the mean Earth’s equator at the reference epoch J2000.0 are denoted with the subscript “eq” in the main text.

G : Newtonian constant of gravitation

c : speed of light in vacuum

ϵ : mean obliquity

ϵ_0 : mean obliquity at the reference epoch J2000.0

$\dot{\epsilon}$: secular rate of the mean obliquity

ζ, ϑ, z : precession angles

ζ_0, z_0 : precession angles at the reference epoch J2000.0

$\dot{\zeta}, \dot{\vartheta}, \dot{z}$: secular rates of the precession angles

$\Delta\psi, \Delta\epsilon$: nutation angles

$A_{\Delta\psi\Omega\zeta}, A_{\Delta\epsilon\Omega\zeta}$: amplitudes of the largest components of the nutation angles $\Delta\psi, \Delta\epsilon$ due to the 18.6-yr lunar motion

M_{\oplus} : mass of the Earth

$\mu_{\oplus} \doteq GM_{\odot}$: gravitational parameter of the Earth

S_{\oplus} : magnitude of the angular momentum of Earth

$\hat{S}_{\oplus} = \{0, \sin \epsilon, \cos \epsilon\}$: spin axis of the Earth in an ecliptic coordinate system

R_{\oplus} : equatorial radius of the Earth

$\overline{C}_{\ell,m}$: fully normalized Stokes coefficient of degree ℓ and order m of the multipolar expansion of the Earth's gravitational potential

$J_{\ell} = -\sqrt{2\ell+1} \overline{C}_{\ell,0}$: zonal harmonic coefficient of degree ℓ of the multipolar expansion of the Earth's gravitational potential

g_{\oplus} : Earth's acceleration of gravity at the equator

$k_{2,1,K_1}^{(0)}$: dimensionless frequency-dependent Love number for the K_1 tidal constituent of degree $\ell = 2$ and order $m = 1$

$H_2^1(K_1)$: frequency-dependent solid tidal height for the K_1 constituent of degree $\ell = 2$ and order $m = 1$

$\delta_{2,1,K_1}$: phase lag of the response of the solid Earth with respect to the constituent K_1 of degree $\ell = 2$ and order $m = 1$.

ρ_w : volumetric ocean water density

k_2' : dimensionless load Love number

$C_{2,1,K_1}^+$: ocean tidal height for the constituent K_1 of degree $\ell = 2$ and order $m = 1$.

$\epsilon_{2,1,K_1}^+$: phase shift due to hydrodynamics of the oceans for the tidal constituent K_1 of degree $\ell = 2$ and order $m = 1$.

\mathbf{r} : satellite's position vector with respect to the Earth

r : magnitude of the satellite's position vector with respect to the Earth

a : semimajor axis of the geocentric satellite's orbit

$n_b \doteq \sqrt{\mu_\oplus a^{-3}}$: Keplerian mean motion of the geocentric satellite's orbit

$P_b \doteq 2\pi n_b^{-1}$: orbital period of the geocentric satellite's orbit

e : eccentricity of the geocentric satellite's orbit

I : inclination of the orbital plane of the geocentric satellite's orbit to the mean ecliptic at the reference epoch J2000.0

Ω : longitude of the ascending node of the geocentric satellite's orbit referred to the mean ecliptic at the reference epoch J2000.0

ω : argument of perigee of the geocentric satellite's orbit referred to the mean ecliptic at the reference epoch J2000.0

$\hat{n} = \{\sin I \sin \Omega, -\sin I \cos \Omega, \cos I\}$: normal unit vector in an ecliptic coordinate system. It is perpendicular to the satellite's orbital plane

M_\odot : mass of the Sun

$\mu_\odot \doteq GM_\odot$: gravitational parameter of the Sun

λ_\odot : ecliptic longitude of the Sun

a_\oplus : semimajor axis of the heliocentric Earth's orbit

$n_b^\oplus \doteq \sqrt{\mu_\odot a_\oplus^{-3}}$: Keplerian mean motion of the heliocentric Earth's orbit

$P_\oplus \doteq 2\pi n_b^{\oplus -1}$: orbital period of the heliocentric Earth's orbit

e_\oplus : eccentricity of the heliocentric Earth's orbit

I_\oplus : inclination of the orbital plane of the heliocentric Earth's orbit to the mean ecliptic at the reference epoch J2000.0

Ω_\oplus : longitude of the ascending node of the heliocentric Earth's orbit referred to the mean ecliptic at the reference epoch J2000.0

M_X : mass of the 3rd body X (Sun \odot or Moon \textcircled{C})

$\mu_X \doteq GM_X$: gravitational parameter of the 3rd body X (Sun \odot or Moon \textcircled{C})

a_X : semimajor axis of the geocentric orbit of the 3rd body X

P_X : orbital period of the geocentric orbit of the 3rd body X

e_X : eccentricity of the geocentric orbit of the 3rd body X

I_X : inclination of the orbital plane of the geocentric orbit of the 3rd body X to the mean ecliptic at the reference epoch J2000.0

Ω_X : longitude of the ascending node of the geocentric orbit of the 3rd body X referred to the mean ecliptic at the reference epoch J2000.0

$\dot{\Omega}_X$: secular rate of the longitude of the ascending node of the geocentric orbit of the 3rd body X referred to the mean ecliptic at the reference epoch J2000.0

$T_{\Omega_{\zeta}}$: period of the node of the geocentric Moon's orbit referred to the mean ecliptic at the reference epoch J2000.0

Appendix B Tables and Figures

Table 1: Relevant physical and orbital parameters used in the text. Most of the reported values come from Iorio (2001); Petit, Luzum & et al. (2010) and references therein. The source for the orbital elements characterizing the heliocentric orbit of the Earth, referred to the mean ecliptic at the reference epoch J2000.0, is the freely consultable database JPL HORIZONS on the Internet at <https://ssd.jpl.nasa.gov/?horizons> from which they were retrieved by choosing the time of writing this paper as input epoch. For the level of accuracy with which some of the parameters listed here are currently known, see the main text.

Parameter	Units	Numerical value
G	$\text{kg}^{-1} \text{m}^3 \text{s}^{-2}$	6.67259×10^{-11}
c	m s^{-1}	2.99792458×10^8
μ_{\oplus}	$\text{m}^3 \text{s}^{-2}$	$3.986004418 \times 10^{14}$
S_{\oplus}	$\text{kg m}^2 \text{s}^{-1}$	5.86×10^{33}
R_{\oplus}	m	6.3781366×10^6
$\overline{C}_{2,0}$	–	$-4.84165299806 \times 10^{-4}$
g_{\oplus}	m s^{-2}	9.7803278
$k_{2,1,K_1}^{(0)}$	–	0.257
$H_2^1(K_1)$	m	0.3687012
$\delta_{2,1,K_1}$	deg	-0.3
ρ_w	kg m^{-3}	1.025×10^3
k_2'	–	-0.3075
$C_{2,1,K_1}^+$	m	2.23659×10^{-2}
$\varepsilon_{2,1,K_1}^+$	deg	315.958
μ_{\odot}	$\text{m}^3 \text{s}^{-2}$	$1.32712440018 \times 10^{20}$
a_{\oplus}	au	1.000003360971446
e_{\oplus}	–	0.01636541170625853
I_{\oplus}	deg	0.003786566401597615
\dot{I}_{\oplus}	deg cty ⁻¹	-0.01337178
Ω_{\oplus}	deg	171.6446280787646
$\dot{\Omega}_{\oplus}$	deg cty ⁻¹	-0.24123856
μ_{ζ}	μ_{\oplus}	$1.23000371 \times 10^{-2}$
a_{ζ}	km	385, 734
e_{ζ}	–	0.05183692147447081
I_{ζ}	deg	5.208682439763778
Ω_{ζ}	deg	125.1041727302047
$\dot{\Omega}_{\zeta}$	// cty ⁻¹	-6, 962, 890.5431
$T_{\Omega_{\zeta}}$	yr	$\simeq 18.6$

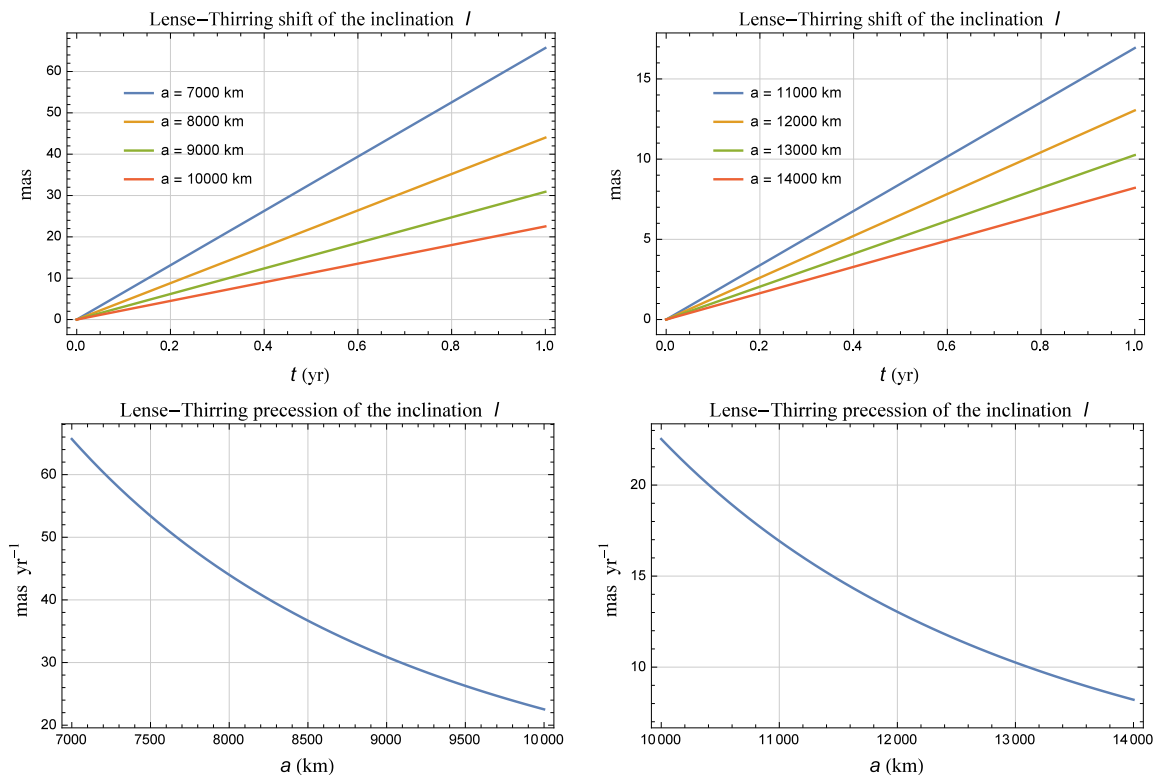


Fig. 1.— Upper row: annual Lense-Thirring shifts of the satellite’s inclination I obtained for different values of a by subtracting two time series produced by numerically integrating the equations of motion in rectangular Cartesian coordinates with and without the gravitomagnetic acceleration. Both the runs shared the same initial conditions characterized, among other things, by $e = 0, \Omega = I = 90$ deg. Lower row: Plot of the Lense-Thirring rate of change of the satellite’s inclination I as a function of the semimajor axis a calculated analytically from Equation (13) for $e = 0, \Omega = I = 90$ deg. In both cases, a reference frame with the mean ecliptic at the epoch J2000.0 was used as reference $\{x, y\}$ plane so that $\hat{S}_x = 0$, $\hat{S}_y = \sin \epsilon = 0.3978$, $\hat{S}_z = \cos \epsilon = 0.9175$.

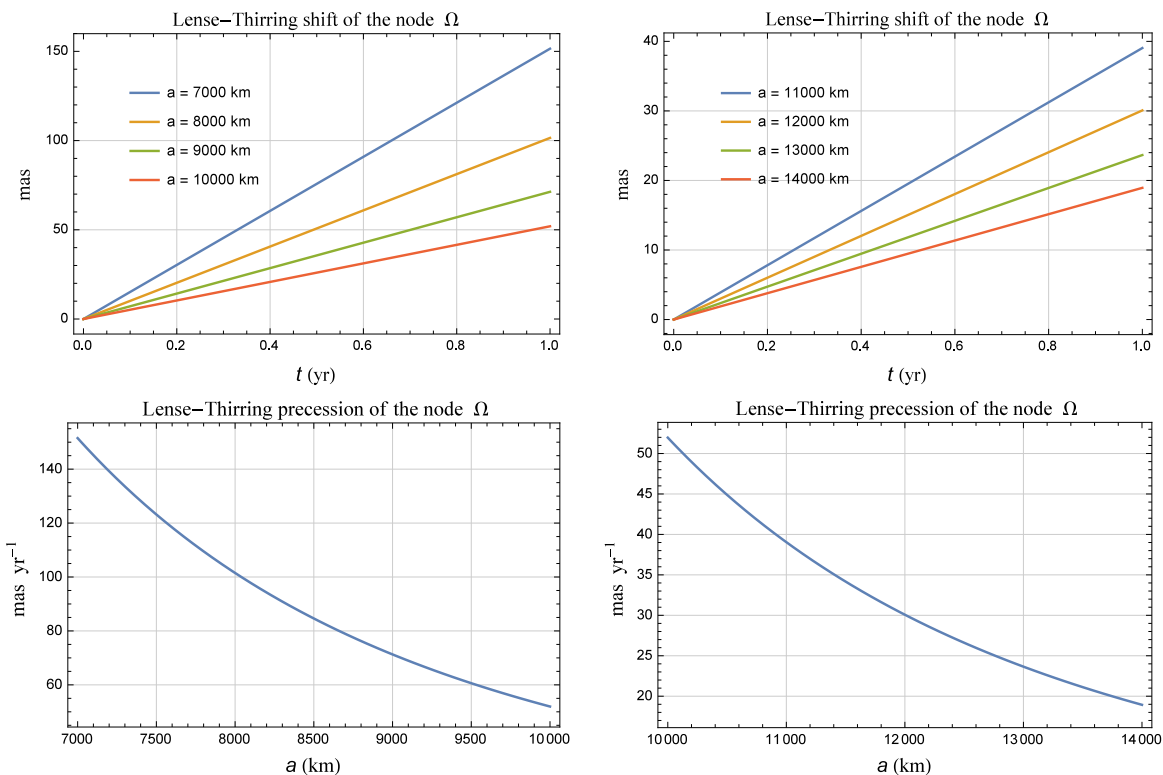


Fig. 2.— Upper row: annual Lense-Thirring shifts of the satellite’s node Ω obtained for different values of a by subtracting two time series produced by numerically integrating the equations of motion in rectangular Cartesian coordinates with and without the gravitomagnetic acceleration. Both the runs shared the same initial conditions characterized, among other things, by $e = 0, \Omega = I = 90$ deg. Lower row: Plot of the Lense-Thirring rate of change of the satellite’s node Ω as a function of the semimajor axis a calculated analytically from Equation (14) for $e = 0, \Omega = I = 90$ deg. In both cases, a reference frame with the mean ecliptic at the epoch J2000.0 was used as reference $\{x, y\}$ plane so that $\hat{S}_x = 0, \hat{S}_y = \sin \epsilon = 0.3978, \hat{S}_z = \cos \epsilon = 0.9175$.

Table 2: Numerical values and associated uncertainties of the relevant astronomical parameters of the precession/nutation and of the obliquity. They were retrieved from Liu & Capitaine (2017) (ϵ_0 , $\dot{\epsilon}$), Capitaine, Wallace & Chapront (2003) (ζ_0 , $\dot{\zeta}$, $\dot{\vartheta}$, z_0 , \dot{z}), Petit, Luzum & et al. (2010) (the amplitudes $A_{\Delta\psi_{\Omega\zeta}}$, $A_{\Delta\epsilon_{\Omega\zeta}}$ of the lunar node terms in $\Delta\psi$, $\Delta\epsilon$).

Parameter	Units	Numerical value	Uncertainty
ϵ_0	"	84,381.411365	8×10^{-6}
$\dot{\epsilon}$	" cty ⁻¹	-460.0836735	1×10^{-7}
ζ_0	"	2.650545	1×10^{-6}
$\dot{\zeta}$	" cty ⁻¹	2,306.083227	1×10^{-6}
$\dot{\vartheta}$	" cty ⁻¹	2,004.191903	1×10^{-6}
z_0	"	-2.650545	1×10^{-6}
\dot{z}	" cty ⁻¹	2,306.077181	1×10^{-6}
$A_{\Delta\psi_{\Omega\zeta}}$	μas	-17,206,424.18	1×10^{-2}
$A_{\Delta\epsilon_{\Omega\zeta}}$	μas	9,205,233.10	1×10^{-2}

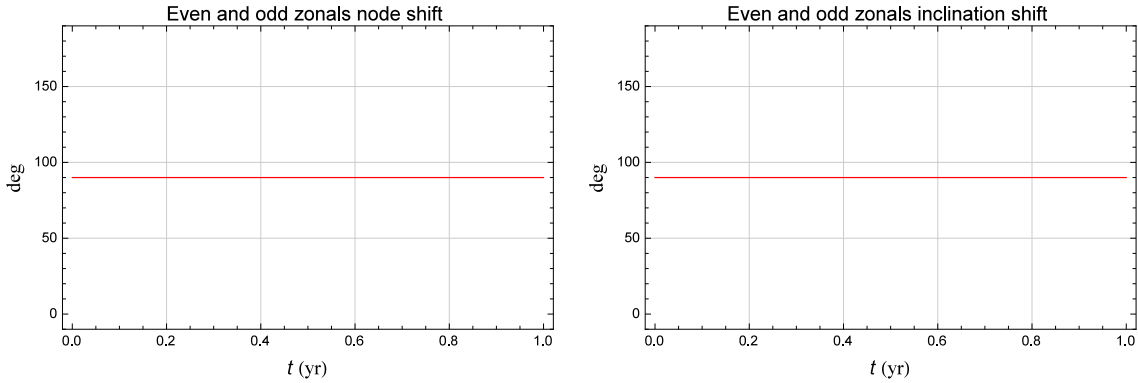


Fig. 3.— Annual shifts of the satellite’s node Ω (left panel) and inclination I (right panel) obtained, for each orbital element, by subtracting two time series produced by numerically integrating the equations of motion in rectangular Cartesian coordinates with and without the classical accelerations due to the first five zonal harmonics J_2 , J_3 , J_4 , J_5 , J_6 of the geopotential. For each orbital element, both the runs shared the same initial conditions characterized, among other things, by $e = 0$, $\Omega = I = 90$ deg. The meaning of the plots displayed is that if the satellite’s node and inclination are set to such initial values, they stay constant to them throughout the orbital evolution. The result turns out to be independent of the semimajor axis a . A reference frame with the mean ecliptic at the epoch J2000.0 was used as reference $\{x, y\}$ plane so that $\hat{S}_x = 0$, $\hat{S}_y = \sin \epsilon = 0.3978$, $\hat{S}_z = \cos \epsilon = 0.9175$.

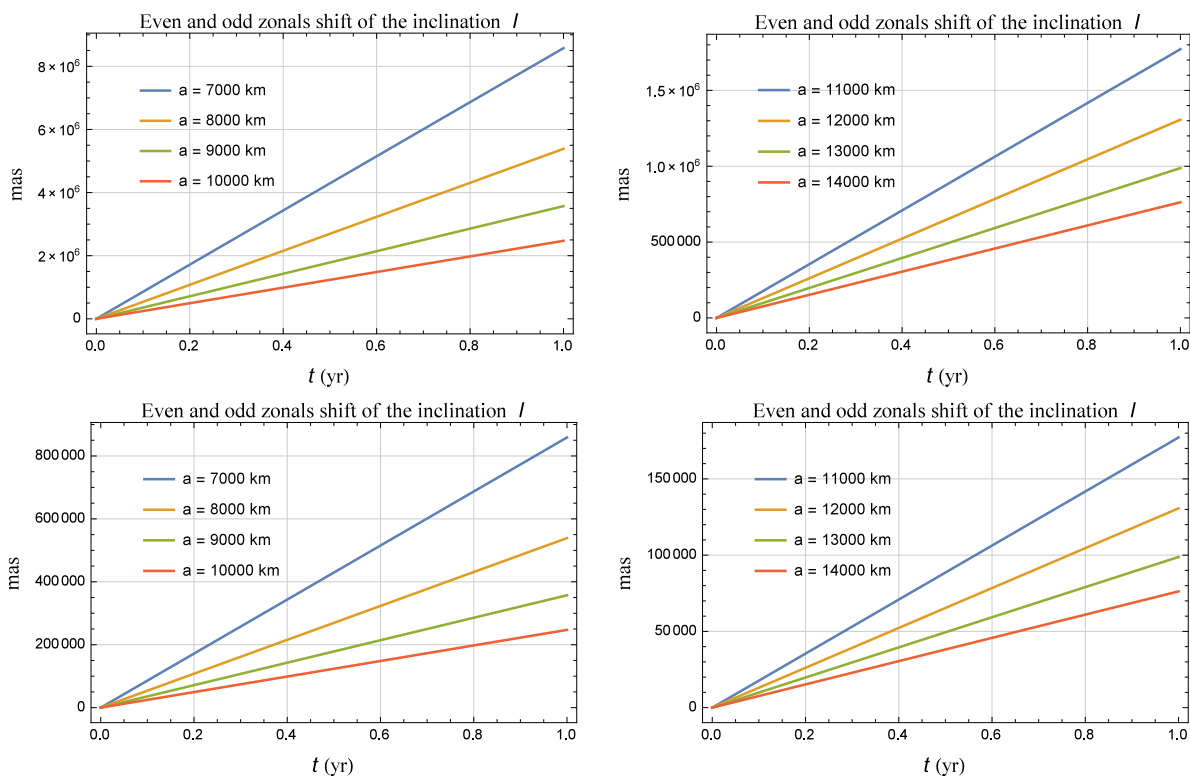


Fig. 4.— Upper row: nominal annual shifts of the satellite’s inclination I obtained for different values of a by subtracting two time series produced by numerically integrating the equations of motion in rectangular Cartesian coordinates with and without the classical accelerations due to the first five zonal harmonics J_2, J_3, J_4, J_5, J_6 of the geopotential. Both the runs shared the same initial conditions characterized, among other things, by $e = 0, \Omega = I = 90 \pm 0.1$ deg. Lower row: same as in the upper row, apart from an offset of 0.01 deg from the ideal condition $I = \Omega = 90$ deg. The largest contribution is due to J_2 , whose present-day uncertainty may be as large as $\lesssim 2 \times 10^{-10}$ if evaluated conservatively; the statistical, formal errors $\sigma_{\bar{C}_{2,0}}$ released in the global gravity field models produced from the GRACE/GOCE data by several institutions around the world are even $\approx 1 - 3$ orders of magnitude smaller. In both cases, a reference frame with the mean ecliptic at the epoch J2000.0 was used as reference $\{x, y\}$ plane so that $\hat{S}_x = 0, \hat{S}_y = \sin \epsilon = 0.3978, \hat{S}_z = \cos \epsilon = 0.9175$.

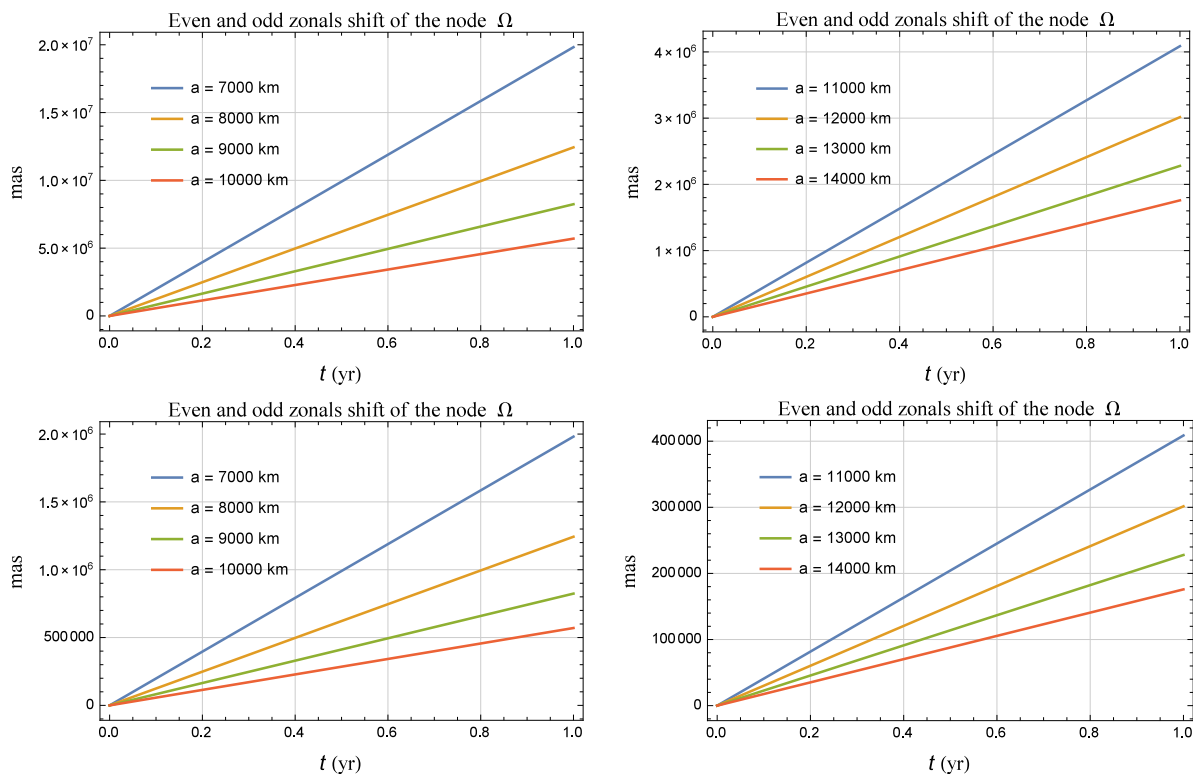


Fig. 5.— Upper row: nominal annual shifts of the satellite’s node Ω obtained for different values of a by subtracting two time series produced by numerically integrating the equations of motion in rectangular Cartesian coordinates with and without the classical accelerations due to the first five zonal harmonics J_2, J_3, J_4, J_5, J_6 of the geopotential. Both the runs shared the same initial conditions characterized, among other things, by $e = 0, \Omega = I = 90 \pm 0.1$ deg. Lower row: same as in the upper row, apart from an offset of 0.01 deg from the ideal condition $I = \Omega = 90$ deg. The largest contribution is due to J_2 , whose present-day uncertainty may be as large as $\lesssim 2 \times 10^{-10}$ if evaluated conservatively; the statistical, formal errors $\sigma_{\bar{C}_{2,0}}$ released in the global gravity field models produced from the GRACE/GOCE data by several institutions around the world are even $\approx 1 - 3$ orders of magnitude smaller. In both cases, a reference frame with the mean ecliptic at the epoch J2000.0 was used as reference $\{x, y\}$ plane so that $\hat{S}_x = 0, \hat{S}_y = \sin \epsilon = 0.3978, \hat{S}_z = \cos \epsilon = 0.9175$.

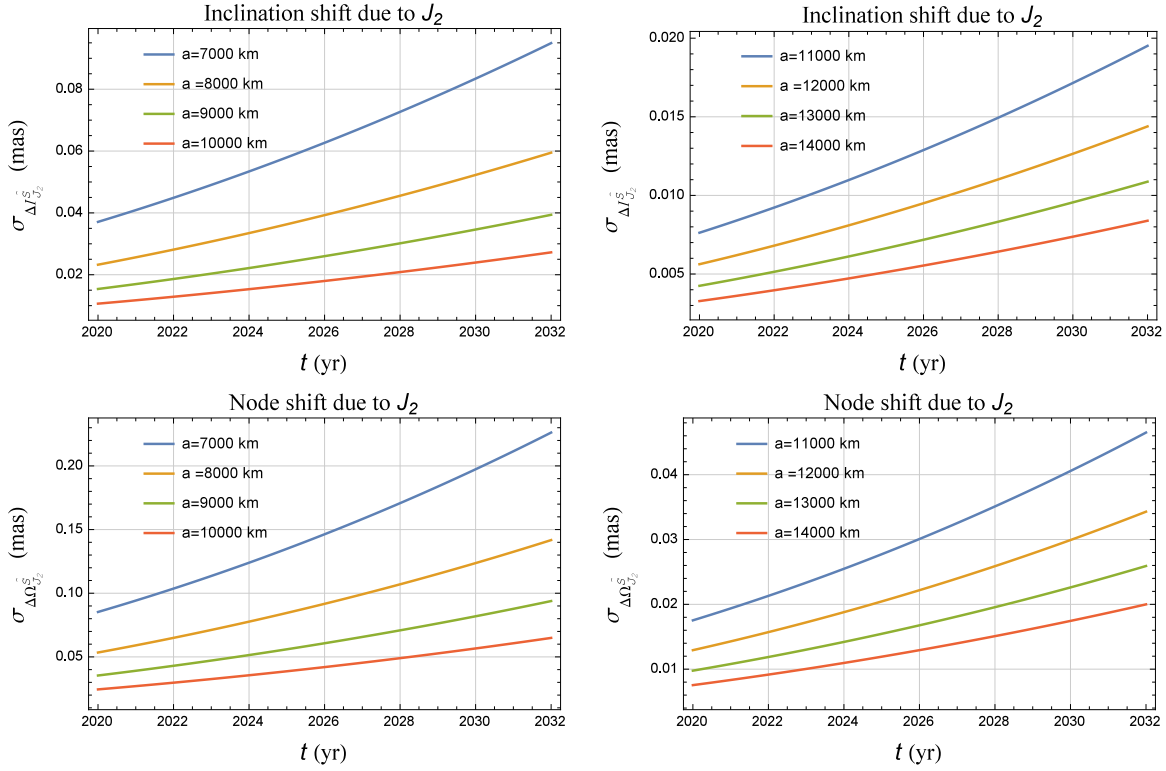


Fig. 6.— Upper row: Mismodeled time series $\sigma_{\Delta I_{J_2}^{\delta}}(t)$, produced analytically from Iorio (2011a, Eqs. (12) to (15)) for different values of the semimajor axis a and $I_0 = \Omega_0 = 90 \pm 0.01$ deg, of the time-dependent J_2 -induced shift of the inclination I due to the uncertainties of the parameters entering the precession/nutation and the temporal change of the obliquity according to the values listed in Table 2 of Appendix B. The nominal value of J_2 , retrieved from some model, was adopted. Lower row: same as for the node.

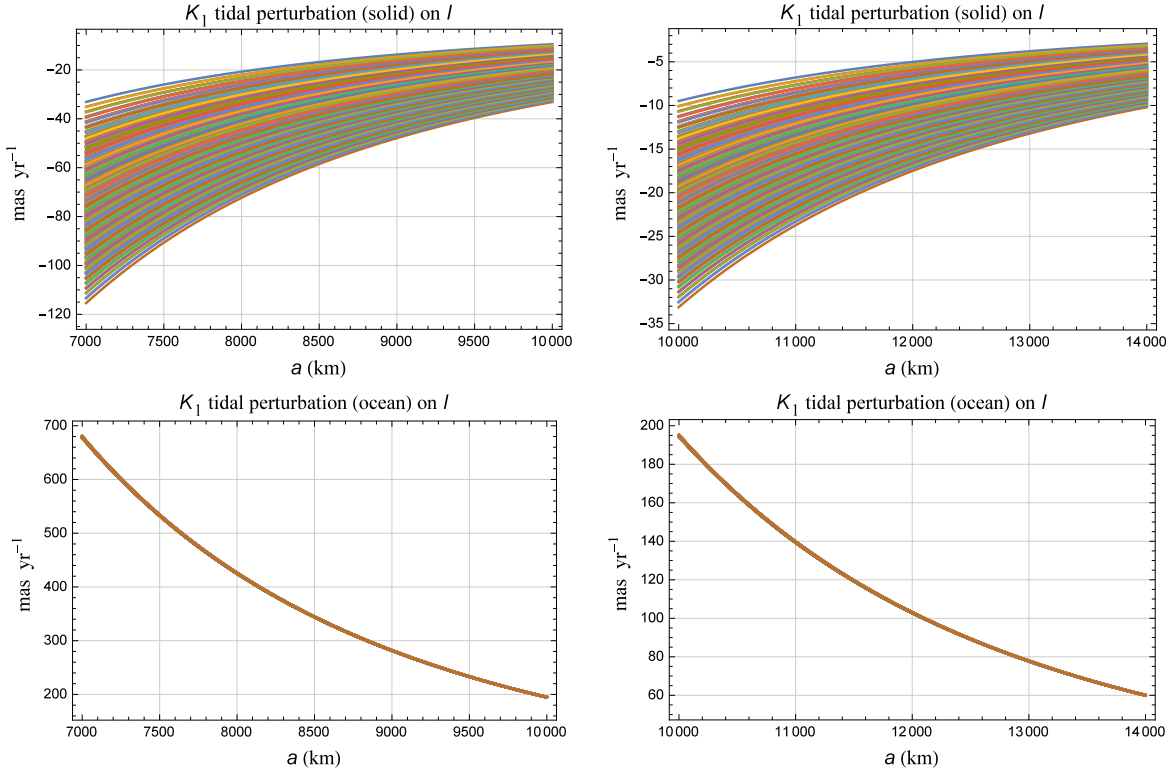


Fig. 7.— Nominal perturbations due to the solid (upper row) and ocean (lower row) component of the $\ell = 2$, $m = 1$, $p = 1$, $q = 0$ constituent of the K_1 tide on the satellite’s inclination I as functions of a , as per Equation (36) and Equation (42). In all the panels, each curve corresponds to a pair of values of I , Ω within the ranges $I = \Omega = 90 \pm 0.05$ deg. The current level of uncertainty in the Love number $k_{2,1,K_1}$ is of the order of $\approx 10^{-3}$ or, perhaps, one order of magnitude better (Jagoda et al. 2018). According to the past EMG96 model (Lemoine et al. 1998), $C_{2,1,K_1}^+$ was known with a relative accuracy of 4×10^{-2} . However, by calculating mean and standard deviation of the values computed at <https://bowie.gsfc.nasa.gov/ggfc/tides/harmonics.html> from the models TPXO.6.2 (Egbert & Erofeeva 2002), GOT99 (Ray 1999) and FES2004 (Lyard et al. 2006), a relative uncertainty of 1.8×10^{-3} is inferred.

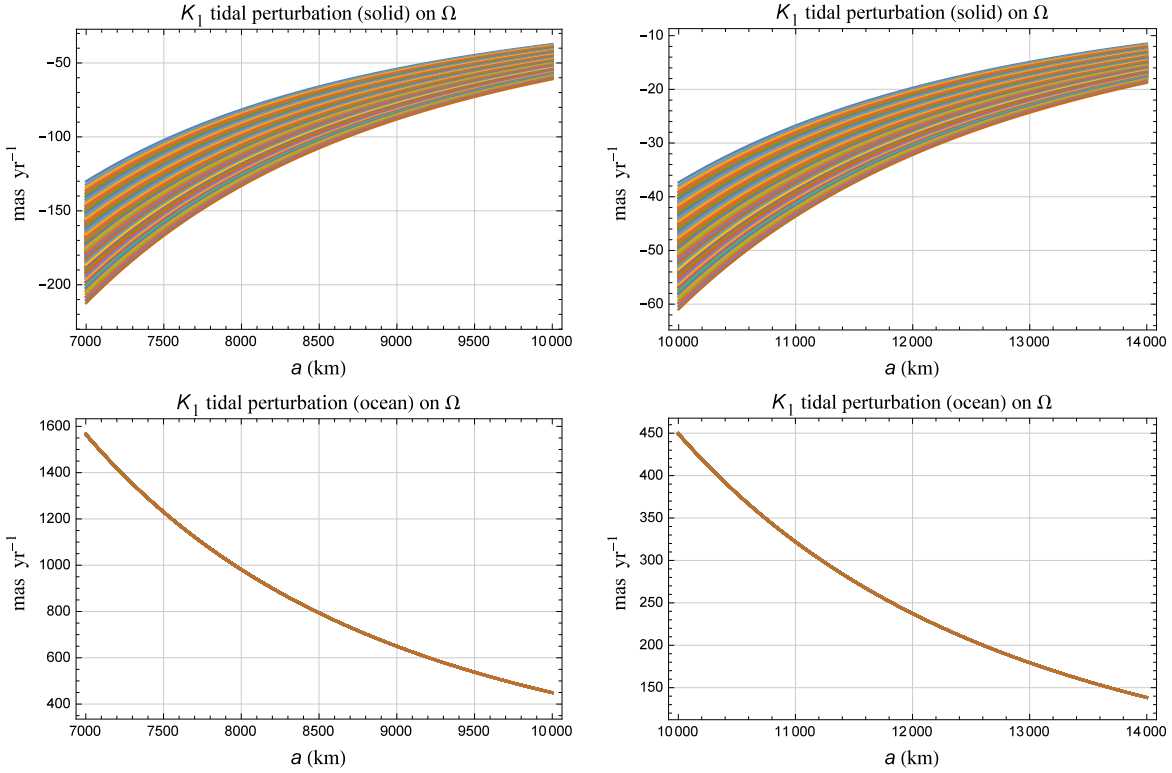


Fig. 8.— Nominal perturbations due to the solid (upper row) and ocean (lower row) component of the $\ell = 2$, $m = 1$, $p = 1$, $q = 0$ constituent of the K_1 tide on the satellite’s node Ω as functions of a , as per Equation (37) and Equation (43). In all the panels, each curve corresponds to a pair of values of I , Ω within the ranges $I = \Omega = 90 \pm 0.05$ deg. The current level of uncertainty in the Love number $k_{2,1,K_1}$ is of the order of $\approx 10^{-3}$ or, perhaps, one order of magnitude better (Jagoda et al. 2018). According to the past EMG96 model (Lemoine et al. 1998), $C_{2,1,K_1}^+$ was known with a relative accuracy of 4×10^{-2} . However, by calculating mean and standard deviation of the values computed at <https://bowie.gsfc.nasa.gov/ggfc/tides/harmonics.html> from the models TPXO.6.2 (Egbert & Erofeeva 2002), GOT99 (Ray 1999) and FES2004 (Lyard et al. 2006), a relative uncertainty of 1.8×10^{-3} is inferred.

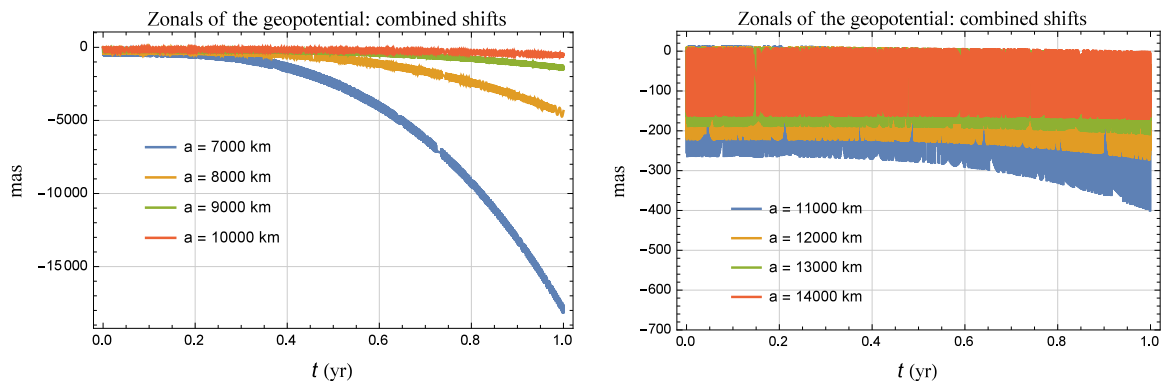


Fig. 9.— Numerically generated nominal amplitudes of the precessions of the satellite’s inclination and node induced by the first five zonal harmonics J_2, J_3, J_4, J_5, J_6 of the geopotential linearly combined according to Equation (46) and Equation (47). They were obtained, for different values of a , by subtracting two time series for the combination of Equation (46) and Equation (47) produced by numerically integrating the equations of motion in rectangular Cartesian coordinates with and without the classical accelerations due to $J_\ell, \ell = 2, 3, 4, 5, 6$. Both the runs shared the same initial conditions characterized, among other things, by $e = 0, \Omega = I = 90 \pm 0.1$ deg. The largest contribution is due to J_2 , whose present-day uncertainty may be as large as $\lesssim 2 \times 10^{-10}$ if evaluated conservatively; the statistical, formal errors $\sigma_{\bar{C}_{2,0}}$ released in the global gravity field models produced from the GRACE/GOCE data by several institutions around the world are even $\approx 1-3$ orders of magnitude smaller. In both cases, a reference frame with the mean ecliptic at the epoch J2000.0 was used as reference $\{x, y\}$ plane so that $\hat{S}_x = 0, \hat{S}_y = \sin \epsilon = 0.3978, \hat{S}_z = \cos \epsilon = 0.9175$.

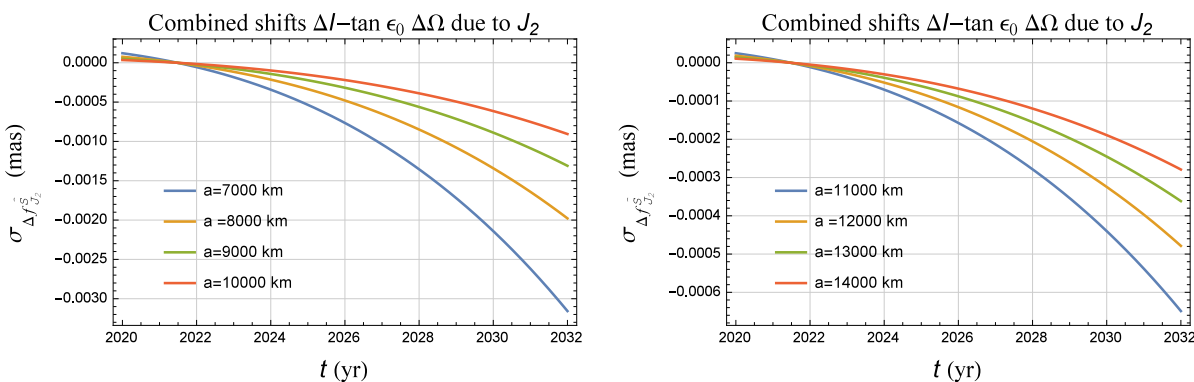


Fig. 10.— Mismodeled combined time series $\sigma_{\Delta J_2^{\hat{s}}}(t)$, produced analytically from Iorio (2011a, Eqs. (12) to (15)) and Equation (46) and Equation (47) for different values of the semimajor axis a and $I = \Omega = 90 \pm 0.01$ deg, of the time-dependent J_2 -induced shifts of the inclination I and the node Ω due to the uncertainties of the parameters entering the precession/nutation and the temporal change of the obliquity according to the values listed in Table 2 of Appendix B. The nominal value of J_2 , retrieved from some model, was adopted.

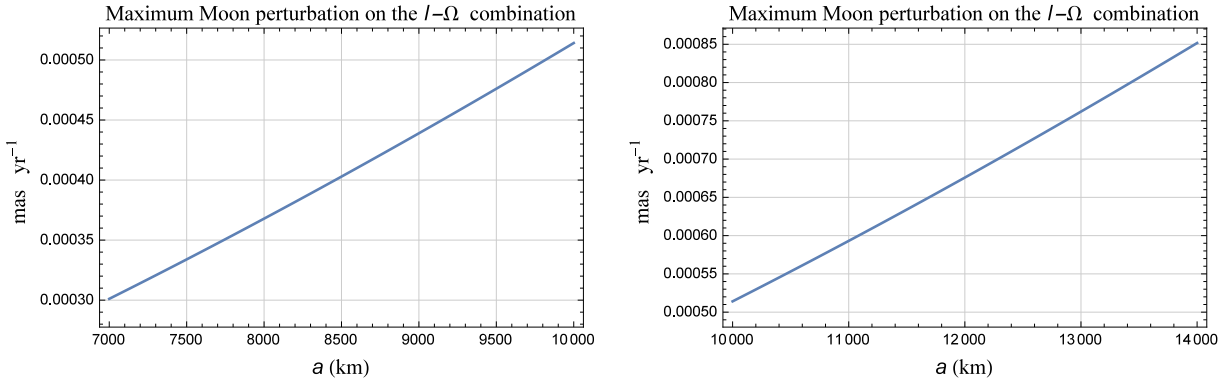


Fig. 11.— Maximum value, in mas yr^{-1} , of the mismodelled part of the 3rd-body precessions of I , Ω due to the Moon combined with Equation (46) and Equation (47) as a function of the satellite’s semimajor axis a ; Equation (56) was used. We assumed a relative uncertainty in $\mu_{\mathcal{L}}$ of 2×10^{-8} , as per the Object Data Page of the Moon provided by the JPL HORIZONS Web interface, revised on 2013.

REFERENCES

- Abdel-Aziz Y. A., Khalil K. I., 2014, *Res. Astron. Astrophys.*, 14, 589
- Bertotti B., Farinella P., Vokrouhlický D., 2003, *Physics of the Solar System*. Kluwer, Dordrecht
- Brumberg V. A., 1991, *Essential Relativistic Celestial Mechanics*. Adam Hilger, Bristol
- Brumberg V. A., Kopeikin S. M., 1989, *Nuovo Cimento B*, 103, 63
- Capitaine N., Wallace P. T., Chapront J., 2003, *Astron. Astrophys.*, 412, 567
- Ciufolini I. et al., 2013, *Nuclear Physics B Proceedings Supplements*, 243-244, 180
- Ciufolini I. et al., 2012a, *Eur. Phys. J. Plus*, 127, 133
- Ciufolini I. et al., 2016, *Eur. Phys. J. C*, 76, 120
- Ciufolini I., Paolozzi A., Pavlis E. C., Ries J. C., Koenig R., Matzner R. A., Sindoni G., Neumayer H., 2009, *Space Sci. Rev.*, 148, 71
- Ciufolini I., Pavlis E. C., Paolozzi A., Ries J., Koenig R., Matzner R., Sindoni G., Neumayer K. H., 2012b, *New Astron.*, 17, 341
- Ciufolini I., Pavlis E. C., Ries J., Koenig R., Sindoni G., Paolozzi A., Neumayer H., 2010, in *Astrophysics and Space Science Library*, Vol. 367, *Astrophysics and Space Science Library*, Ciufolini I., Matzner R. A. A., eds., p. 371
- Damour T., Soffel M., Xu C., 1994, *Phys. Rev. D*, 49, 618
- de Sitter W., 1916, *Mon. Not. Roy. Astron. Soc.*, 77, 155
- Dickey J. O. et al., 1994, *Science*, 265, 482
- Eanes R., Schuler A., 1999, in *EGS 24th General Assembly*, Hague, Netherlands
- Egbert G. D., Erofeeva S. Y., 2002, *J. Atmos. Oceanic Tech.*, 19, 183
- Everitt C. W. F., Buchman S., Debra D. B., Keiser G. M., Lockhart J. M., Muhlfelder B., Parkinson B. W., Turneure J. P., 2001, in *Lecture Notes in Physics*, Berlin Springer Verlag, Vol. 562, *Gyros, Clocks, Interferometers ...: Testing Relativistic Gravity in Space*, Lämmerzahl C., Everitt C. W. F., Hehl F. W., eds., p. 52
- Everitt C. W. F. et al., 2011, *Phys. Rev. Lett.*, 106, 221101
- Everitt C. W. F. et al., 2015, *Classical Quant. Grav.*, 32, 224001
- Felsentreger T. L., Marsh J. G., Agreen R. W., 1976, *J. Geophys. Res.*, 81, 2557

- Ferraz Mello S., 1972, *Celest. Mech. Dyn. Astr.*, 5, 80
- Fokker A. D., 1920, *Versl. Kon. Ak. Wet.*, 29, 611
- Hofmann F., Müller J., 2018, *Classical Quant. Grav.*, 35, 035015
- Iorio L., 2001, *Celest. Mech. Dyn. Astr.*, 79, 201
- Iorio L., 2011a, *Phys. Rev. D*, 84, 124001
- Iorio L., 2011b, *Europhys. Lett.*, 96, 30001
- Iorio L., 2012a, *J. High Energy Phys.*, 5, 73
- Iorio L., 2012b, *Celest. Mech. Dyn. Astr.*, 112, 117
- Iorio L., 2017, *Eur. Phys. J. C*, 77, 73
- Iorio L., 2018, arXiv:1809.01730
- Iorio L., Lichtenegger H. I. M., Ruggiero M. L., Corda C., 2011, *Astrophys. Space Sci.*, 331, 351
- Jagoda M., Rutkowska M., Kraszewska K., Suchocki C., 2018, *Stud. Geophys. Geod.*
doi:10.1007/s11200-018-0610-8, at press, 1
- Kahn R., 2007, *The Gravity Probe B Experiment. “Testing Einstein’s Universe”. Post Flight Analysis-Final Report.* Stanford University
- Kopeikin S., Efroimsky M., Kaplan G., 2011, *Relativistic Celestial Mechanics of the Solar System.* Wiley-VCH, Weinheim
- Lemoine F. G. et al., 1998, *The Development of the Joint NASA GSFC and the National Imagery and Mapping Agency (NIMA) Geopotential Model EGM96.* NASA/TP-1998-206861. Goddard Space Flight Center, Greenbelt
- Lense J., Thirring H., 1918, *Physikalische Zeitschrift*, 19, 156
- Lerch F. J. et al., 1992, *Geopotential models of the Earth from satellite tracking, altimeter and surface gravity observations: GEM-T3 and GEM-T3S.* NASA Technical Memorandum 104555. Goddard Space Flight Center, Greenbelt
- Lhotka C., Celletti A., Galeş C., 2016, *Mon. Not. Roy. Astron. Soc.*, 460, 802
- Liu J.-C., Capitaine N., 2017, *Astron. Astrophys.*, 597, A83
- Lucchesi D. M., 2001, *Planet. Space Sci.*, 49, 447
- Lucchesi D. M., 2002, *Planet. Space Sci.*, 50, 1067

- Lucchesi D. M., Anselmo L., Bassan M., Pardini C., Peron R., Pucacco G., Visco M., 2015, *Classical Quant. Grav.*, 32, 155012
- Lyard F., Lefevre F., Letellier T., Francis O., 2006, *Oc. Dyn.*, 56, 394
- Mayer-Gürr T., Savcenko R., Bosch W., Daras I., Flechtner F., Dahle C., 2012, *J. Geodyn.*, 59, 28
- Milani A., Nobili A., Farinella P., 1987, *Non-gravitational perturbations and satellite geodesy*. Adam Hilger, Bristol
- Montenbruck O., Gill E., 2000, *Satellite Orbits*. Springer-Verlag, Berlin Heidelberg
- Murray C. D., Dermott S. F., 2000, *Solar System Dynamics*. Cambridge University Press
- Petit G., Luzum B., et al., 2010, *IERS Technical Note*, 36, 1
- Pitjeva E. V., 2015, *J. Phys. Chem. Ref. Data*, 44, 031210
- Poisson E., Will C. M., 2014, *Gravity*. Cambridge University Press, Cambridge
- Pucacco G., Lucchesi D. M., 2018, *Celest. Mech. Dyn. Astr.*, 130, 66
- Pugh G., 1959, *Proposal for a Satellite Test of the Coriolis Prediction of General Relativity*. Research Memorandum 11, Weapons Systems Evaluation Group, The Pentagon, Washington D.C.
- Ray R., 1999, *A global ocean tide model from topex/poseidon altimetry: Got99*. NASA Technical Memorandum NASA/TM209478, Goddard Space Flight Center, Greenbelt, USA
- Renzetti G., 2012, *Can. J. Phys.*, 90, 883
- Renzetti G., 2013a, *New Astron.*, 23, 63
- Renzetti G., 2013b, *Central European Journal of Physics*, 11, 531
- Renzetti G., 2013c, *J. Astrophys. Astron.*, 34, 341
- Renzetti G., 2014a, *Astrophys. Space Sci.*, 352, 493
- Renzetti G., 2014b, *New Astron.*, 29, 25
- Renzetti G., 2015, *Acta Astronaut.*, 113, 164
- Savcenko R., Bosch W., 2012, *EOT11a-Empirical ocean tide model from multi-mission satellite altimetry*. Deutsches Geodätisches Forschungsinstitut, München
- Schaechter D., Breakwell J. V., van Patten R. A., Everitt C. W. F., 1977, *J. Spacecraft Rockets*, 14, 474

- Schaechter D., Breakwell J. V., van Patten R. A., Everitt F. W., 1976, *J. Astronaut. Sci.*, 24, 137
- Schiff L., 1960, *Physical Review Letters*, 4, 215
- Schouten W. J. A., 1918, *Versl. Kon. Ak. Wet.*, 27, 214
- Sehna L., 1981, *Celest. Mech. Dyn. Astr.*, 25, 169
- Soffel M. et al., 2003, *AJ*, 126, 2687
- van Patten R. A., Breakwell J. V., Schaechter D., Everitt C. W. F., 1978, *Acta Astronaut.*, 5, 77
- van Patten R. A., Everitt C. W. F., 1976a, *Celest. Mech. Dyn. Astr.*, 13, 429
- van Patten R. A., Everitt C. W. F., 1976b, *Phys. Rev. Lett.*, 36, 629
- Visco M., Lucchesi D. M., 2016, *Adv. Space Res.*, 57, 1928
- Visco M., Lucchesi D. M., 2018, *Phys. Rev. D*, 98, 044034
- Wagner C. A., McAdoo D. C., 2012, *J. Geodesy*, 86, 99
- Williams J. G., Turyshev S. G., Boggs D. H., 2004, *Phys. Rev. Lett.*, 93, 261101